JGR Atmospheres

RESEARCH ARTICLE
10.1029/2023JD039694

Dust Source Activation Frequency in the Horn of Africa

Tereza Kunkelova[1], Anya J. Crocker[1], Paul A. Wilson[1], and Kerstin Schepanski[2]

[1]University of Southampton, Waterfront Campus, National Oceanography Centre, Southampton, UK, [2]Free University of Berlin, Institute of Meteorology, Berlin, Germany

Key Points:

- High-resolution dust activation map of the Horn of Africa (HoA) using Meteosat Second Generation Spinning Enhanced Visible and Infrared Imager dust index images
- Dust activation extends to unusually low latitudes in the HoA and is unusually seasonal, with most occurring during boreal summer
- The Afar Triangle is, by far, the most active dust source in the HoA accounting for 77.1% of all recorded events

Supporting Information:

Supporting Information may be found in the online version of this article.

Correspondence to:

T. Kunkelova,
tereza.kunkelova@soton.ac.uk

Citation:

Kunkelova, T., Crocker, A. J., Wilson, P. A., & Schepanski, K. (2024). Dust source activation frequency in the Horn of Africa. *Journal of Geophysical Research: Atmospheres*, *129*, e2023JD039694. https://doi.org/10.1029/2023JD039694

Received 4 AUG 2023
Accepted 11 DEC 2023

Author Contributions:

Conceptualization: Anya J. Crocker, Paul A. Wilson, Kerstin Schepanski
Data curation: Tereza Kunkelova
Formal analysis: Tereza Kunkelova
Methodology: Tereza Kunkelova
Resources: Paul A. Wilson, Kerstin Schepanski
Supervision: Anya J. Crocker, Paul A. Wilson, Kerstin Schepanski
Visualization: Tereza Kunkelova
Writing – original draft: Tereza Kunkelova, Anya J. Crocker, Paul A. Wilson, Kerstin Schepanski

Abstract Mineral dust aerosols play an important role in Earth's climate through interactions with incoming solar radiation, clouds, and the atmosphere. However, dust sources in the Horn of Africa (HoA) and controls on their activation are poorly documented. Here, we use fifteen-minute Meteosat Second Generation Spinning Enhanced Visible and Infrared Imager dust index images to identify HoA dust source areas and to quantify their activation frequency in 1° × 1° resolution from 2006 to 2010. Around half of all recorded dust events occur in boreal summer, mostly between 8:00 and 16:00 local time. They are driven by meso- to regional scale meteorological mechanisms including the breakdown of the nocturnal low-level jets, land-sea breezes, and haboobs. By far the most dust-active region in the HoA is the Afar Triangle (>77% of all recorded dust events) which features the Afar and Danakil depressions and is fed by the Awash River. Despite experiencing strong and persistent southwest summer monsoon winds, dust activation on the Somali Peninsula is less significant. A composite of our map with data for North Africa and westernmost Asia shows that the HoA is a striking latitudinal anomaly with dust activation extending deep into the equatorial belt. Our data also reveal that dust activation is unusually seasonal with ∼40% of events occurring in June and July. Our findings show that aridity and mean wind strength alone are poor predictors of dust activation and underscore the strong control exerted by the availability of readily deflated unconsolidated riverine and lacustrine sediments.

Plain Language Summary Mineral dust aerosols play an important role in Earth's climate through interactions with incoming solar radiation, clouds, and processes in the atmosphere. North Africa is the biggest contributor of mineral dust to global atmospheric loading and dust activation is relatively well understood. However, the dust activation in the Horn of Africa (HoA) is currently poorly documented. We use high-resolution remote sensing imagery to identify main dust hot spots in this region over 4 years. Dust activation primarily occurs throughout the day during boreal summer and is driven by medium to regional scale meteorological mechanisms. By far the most dust-active region is the Afar Triangle, which features the lower Awash River system and the Afar and Danakil depressions. Dust activation within the Somali Peninsula is less significant. A composite of our data together with data for North Africa and westernmost Asia reveals a striking latitudinal anomaly. Modern day dust activation in the northern hemisphere is typically confined to latitudes north of ∼13°N but in the HoA, it extends deep into the equatorial belt. Our findings show that aridity and wind strength are poor predictors of dust activation, highlighting the strong control exerted by the availability of dried surface sediments.

1. Introduction

Mineral dust is the main contributor to atmospheric aerosol loading and plays an important role in Earth's climate system. The global radiation budget is both directly and indirectly affected by the interaction of aerosol particles through back-scattering, absorption and re-emission of radiation flux (Shao et al., 2011; Sokolik & Toon, 1996; Sokolik et al., 2001). Aerosols also impact the hydrological cycle by influencing cloud formation processes, serving as condensation nuclei which enhance ice crystal and cloud droplet formation, altering cloud optical properties, and precipitation amounts (Alizadeh-Choobari et al., 2014; Lohmann & Feichter, 2005; Wurzler et al., 2000). Mineral dust also provides macro and micro-nutrients to ocean and terrestrial ecosystems, influencing the carbon and nitrogen cycles by driving marine phytoplankton growth in nutrient-limited regions (e.g., Jickells et al., 2005). In high concentrations mineral dust can lead to debilitating-to-lethal human health outcomes and can cause road and air traffic closures (Esmaeil et al., 2014; Tam et al., 2012).

The sensitivity of the dust cycle to changes in Earth's climate is evident in palaeoclimate records from ocean sediment cores which identify a strong response to insolation forcing on astronomical timescales (e.g., Clemens et al., 1996; deMenocal, 2004). We now know that these astronomically controlled shifts between humid and dry

Writing – review & editing: Tereza Kunkelova, Anya J. Crocker, Paul A. Wilson, Kerstin Schepanski

dusty conditions are long-lived on Africa, pre-dating both the inception of the Plio-Pleistocene ice ages and the development of bipedalism in our hominid ancestors by many millions of years (Crocker et al., 2022). Furthermore, palaeoclimate records reveal that North Africa was periodically even dustier than present in the recent geological past (e.g., Crocker et al., 2022; deMenocal, 1995; McGee et al., 2013; Mulitza et al., 2008). However, the response of the global dust cycle to ongoing human-driven climate change is uncertain (e.g., Huneeus et al., 2011; Kok et al., 2018; Mahowald, 2007; Tegen et al., 2004; Woodward et al., 2005; Wu et al., 2020).

Among the main factors influencing aerosol dust loading today are the geomorphological and atmospheric processes that control deflation and atmospheric entrainment. In regions where detailed information is available, such as North Africa, palaeo-alluvial deposits in arid to semi-arid regions such as dried out stream and lake beds, as well as flood deposits in ephemeral rivers and lake systems, act as hotspots of atmospheric dust emissions (e.g., Bakker et al., 2019; Washington et al., 2003, 2006). Rich in unconsolidated fine silts and clays with sparse to no vegetation cover, these environments provide the ideal surface conditions for wind-driven entrainment and lofting into the atmosphere (Ginoux et al., 2012). However, in many dust-producing regions, field studies are sparse because of the vast areas to cover and/or the geopolitical challenges in some regions. Remotely sensed data therefore provide an effective way of mapping the sources of dust activation and its transport pathways once entrained into the atmosphere.

Early work with remote sensing data revealed that atmospheric dust loading globally is dominated by sources in the Northern Hemisphere with a prominent "dust belt" stretching from western North Africa through the Arabian Peninsula deep into Central Asia (e.g., Carlson, 1979; Prospero, 1981). Since these early studies, subsequent work, benefiting from improved temporal and spatial resolution, has led to more granularity of understanding. Radiance measurements from the Total Ozone Mapping Spectrometer (TOMS) and Ozone Monitoring Instrument have been used to obtain daily maps of absorbing aerosol index (AAI) showing dust aerosol over deserts (Herman et al., 1997; Prospero et al., 2002; Torres et al., 2007). Sensors measuring visible (deep blue) wavelengths, available from Moderate Resolution Imaging Spectroradiometer (MODIS) and Sea-viewing Wide Field-of-view Sensor (SeaWiFS) have provided information on aerosol properties over bright desert surfaces (Ginoux et al., 2012; Hsu et al., 2004) while infrared (IR) spectra Difference Dust Index (IDDI) from Meteosat records have yielded daily nearly noon-time dust source area information (Brooks & Legrand, 2000). However, the temporal resolution of these data sets is limited to one measurement per day (or two if combining MODIS flying on the Terra and Aqua satellites) at fixed local times. This is a fundamental problem for accurate mapping because dust mobilization is triggered by meteorological events at synoptic-, meso-, and local scales resulting in inherent variability of events in time as well as space. Thus, a single measurement per day leads to a transport bias in estimates of mean aerosol distributions and properties and falsely identifies dust sources above areas located downwind of dust active regions. To address these problems, Schepanski et al. (2007) developed a method to identify dust emission sources from high-resolution images collected every 15 min from the Meteosat Second Generation (MSG) Spinning Enhanced Visible and Infrared Imager (SEVIRI). This method has been used to develop quantitative maps of modern dust source activation frequency (DSAF) for North Africa (Schepanski et al., 2012 and references therein) and for the Arabian Peninsula and southwest Asia (Hennen, 2017): see Kunkelova et al. (2022) for a composite of Northeast Africa and Western Asia. Here, we apply the same approach to present the first high-resolution DSAF map for the HoA (39°E, 14°N to 52°E, 5°S), providing unprecedented spatial and temporal quantification of dust activation in a region characterized by strong variability in rainfall at seasonal to geological timescales, and where the response of hydroclimate to future human-driven warming is uncertain.

2. Background

2.1. Dust Activation in the Horn of Africa

Previous studies using remotely sensed data have identified the Horn of Africa (HoA) as an important dust-active region (Ginoux et al., 2012; Prospero et al., 2002; Figure 1). However, there are major discrepancies between studies in the dust sources identified. Prospero et al. (2002) report high AAI values (measured by TOMS) over a broad region of Danakil-Afar and the northern Somali coast with the highest values in the northern end of the Danakil Depression, centered over the intermittent Asake Lake (Prospero et al., 2002; Figure 1a) (see Figures 2b and 2c for locations mentioned in text). Ginoux et al. (2012) identified several localized dust sources in the Danakil Depression using dust optical depth (DOD) data acquired from the MODIS DeepBlue Level 2 (M-DB2) aerosol

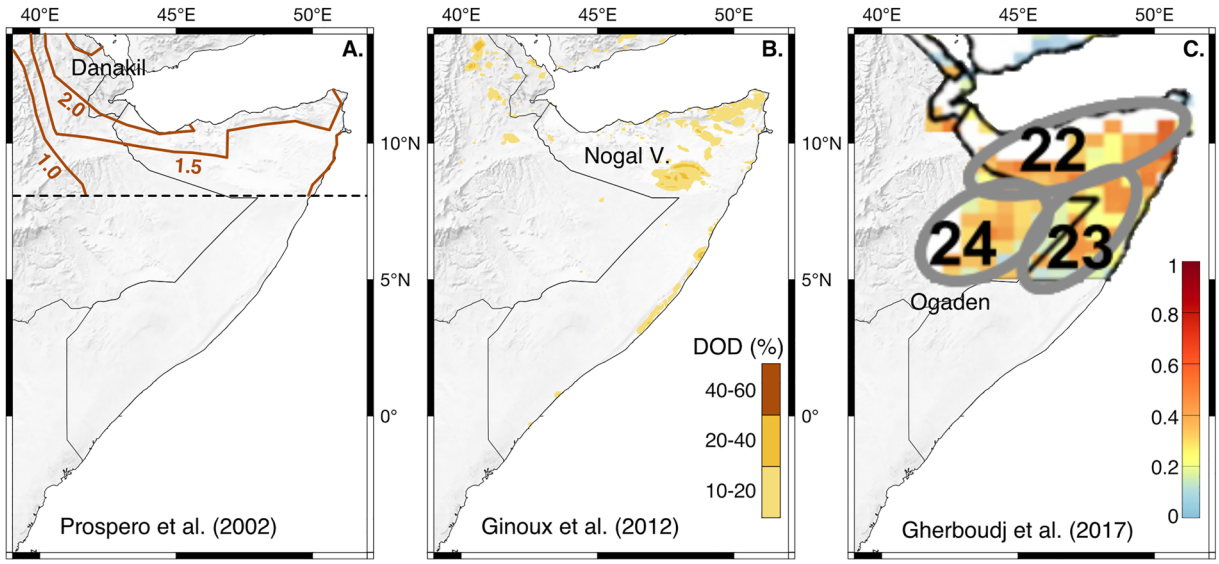

Figure 1. Comparison of different published estimates of dust activity for the Horn of Africa (Gherboudj et al., 2017; Ginoux et al., 2012; Prospero et al., 2002). (a) Mean values of Total Ozone Mapping Spectrometer absorbing aerosol index for July 1986 plotted as isolines (brown line) (adapted from Prospero et al. (2002)). The latitudinal limit of data presented by this study is shown by black dashed line. (b) Frequency levels of distribution of the number of days per season (March, April, and May) of M-DB2 dust optical depth > 0.2 between 2003 and 2009 shown in % (Ginoux et al., 2012). (c) Modeled annual dust emission map based on hourly simulated sandblasting simulations between 2011 and 2014, higher modeled dust fluxes shown in warmer colors (from Gherboudj et al. (2017)). Numbered areas represent the dust source regions as defined by Gherboudj et al. (2017). Region number 22 depicts the Nogal valley, 23 covers the Somalia coastal deserts, and 24 indicates the Ogaden desert region (see Table 2 in Gherboudj et al. (2017) for more details).

product, but they also identify two dust-producing regions in Somalia: (a) a desert strip along the south-eastern coast and (b) the northwest-southeast trending Nogal Valley (Ginoux et al., 2012; Figure 1b). To some extent these discrepancies may be attributed to technical reasons: (a) the TOMS-AAI and M-DB2 DOD data sets are of different spatial resolutions (50 and 10 km^2, respectively) and (b) the TOMS data are insensitive to aerosols in the boundary layer (Torres et al., 1998, 2002) meaning that dust emissions below 500–1,000 m are unlikely to be detected. However, it is likely that an even bigger factor is data coverage through time: the DOD frequency data of Ginoux et al. (2012) cover a six year period (2003–2009) and show that peak dust activation occurs during a large portion of the year (March through August) while analysis shown of the HoA by Prospero et al. (2002) is limited to a single example month (July 1986).

Gherboudj et al. (2017) modeled regional dust sources by simulating sandblasting fluxes between 2011 and 2014 using wind speed and ground surface variables (soil moisture, roughness, vegetation index, clay/sand fraction, soil erodibility and texture). Their simulations suggested that dust was generated across almost all of northern Somalia (with the exception of the coastal region) and easternmost Ethiopia, with the Ogaden desert in eastern Ethiopia and the Nogal valley identified as the main dust producing hotspots. Highest dust emission fluxes were identified during the summer (June–August). Contrary to the AAI and DOD data, the sandblasting model did not identify the Danakil Depression as an important dust source (Figure 1c). These simulations were limited by the low resolution of the climatic variables used, particularly the wind speed data (~75 km), making the approach unsuitable to simulating meso- and regional scale dust emissions, such as haboob dust storm events (Gherboudj et al., 2017). Thus, areas that experience climatic phenomena occurring at scales of less than 100 km do not appear as dust hot spots in the resulting maps of simulated dust generation.

2.2. Regional Climate and Meteorology

The HoA is the easternmost region of the African continent, and comprises eastern Ethiopia, Eritrea, Djibouti, Somalia, and northeast Kenya. The region is characterized by strong spatial and seasonal variations in precipitation, temperatures and wind pattern. Herein, we define the HoA as a region from 39°E, 5°S to 52°E, 14°N (Figures 2b and 2c). The northernmost HoA includes north-eastern Ethiopia, southern Eritrea and Djibouti and here, the complex topography with contrasting landscapes, such as the Danakil and Afar depressions bound by the mountains of the East African Rift (the Ethiopian Highlands and Ahmar Mountains), results in greatly

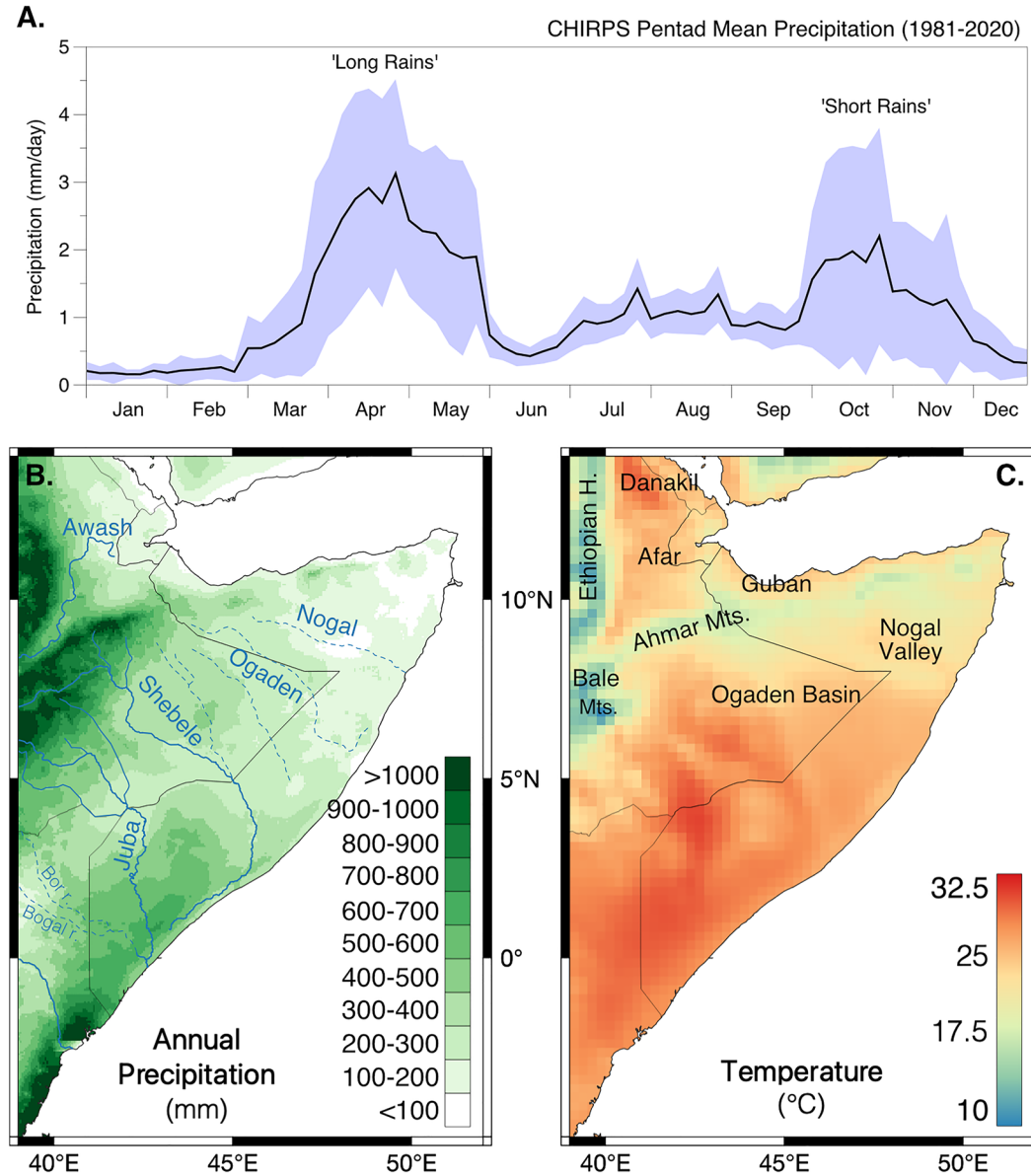

Figure 2. Seasonality of rainfall and mean annual precipitation and surface air temperature over the Horn of Africa (HoA). (a) 40-year record of monthly mean precipitation rates from Climate Hazards Group InfraRed Precipitation with Station (CHIRPS) pentad (5-day) data from 1 January 1981 to 1 January 2021 (Funk et al., 2015); black line represents the mean value across the HoA region (39–52°E, 14°N–5°S) with ± one standard deviation shown in blue. (b) Spatial distribution of annual mean precipitation between January 1981 and December 2020 from CHIRPS pentad data set (Funk et al., 2015). Blue lines show active rivers, blue dashed lines represent seasonal "wadi" rivers with drainage basin names in blue, Bor and Bogal seasonal rivers in northeast Kenya are labeled with light blue. (c) Mean annual temperature (January 1981 to December 2020) from European Centre for Medium-Range Weather Forecasts Reanalysis 5 (ECMWF ERA5) data set (Muñoz Sabater, 2019); black labels show key high elevation mountain ranges as well as lowlands and depressions. Country boundaries in gray. Data generated using Google Earth Engine (GEE).

varied climatological conditions from hot and hyperarid to cooler alpine climates (Figures 2b and 2c). The southern HoA consists of eastern Ethiopia, Somalia and eastern Kenya and here, regional climate variability is less pronounced over predominantly flat terrain with a gentle incline toward the Indian Ocean south of the Ahmar Mountains (Figures 2b and 2c).

Over seasonal timescales, climate in the HoA is strongly influenced by latitudinal migration of the tropical rain belt (TRB). During boreal winter, the TRB is located to the south (~10°S) and most of the region experiences

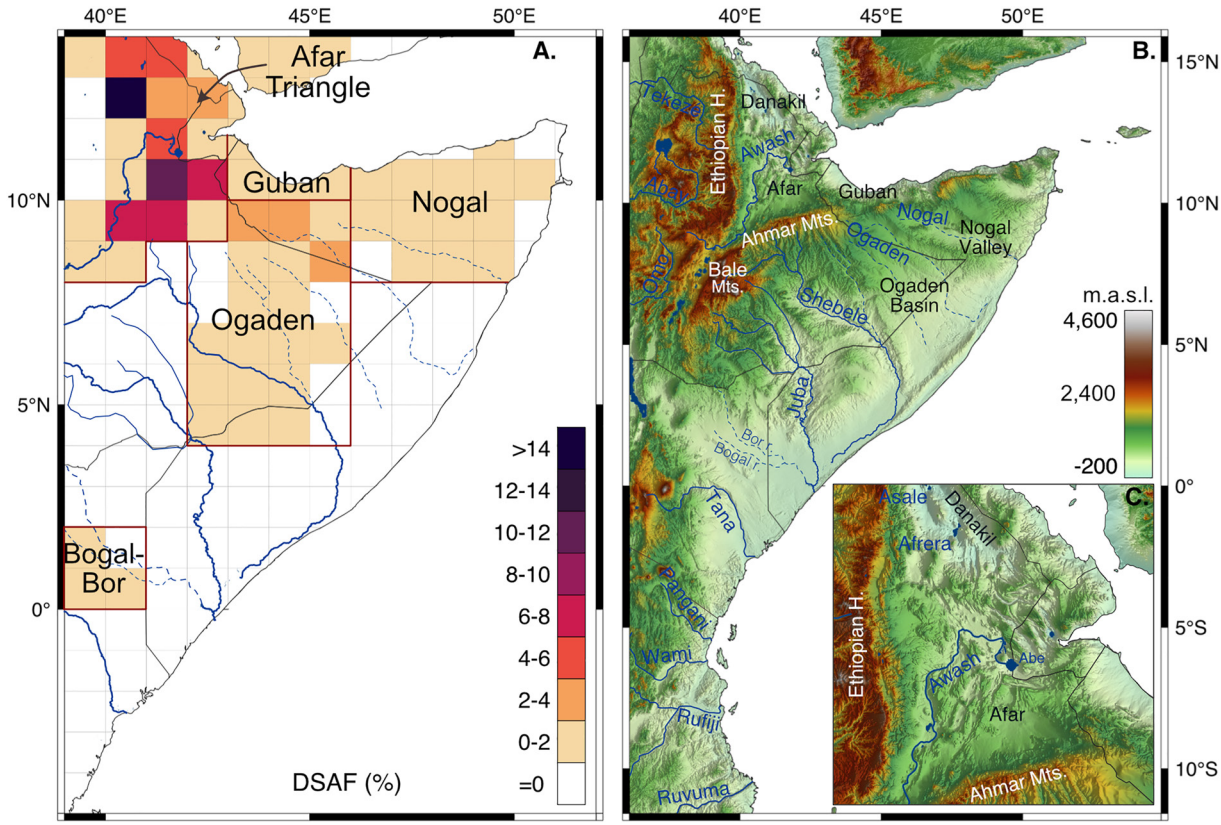

Figure 3. (a) Our new multi-annual dust source activation frequency (in %) map of the Horn of Africa. Five dust-active regions labeled with boundaries shown by red lines: Afar Triangle, Ogaden, Nogal, Bogal-Bor, and Guban. Four-year observation interval: March 2006 to February 2010. Rivers and lakes in dark blue. (b) Regional topography (m.a.s.l.) using a 30 arc-second (approx. 1 km at the equator) resolution Digital Elevation Model from the Shuttle Radar Topography Mission (Lehner et al., 2008); rivers and lakes are labeled in blue, national boundaries in dark gray, mountains in white and valleys, basins and depressions in black. Inset shows the Afar Triangle region.

north-easterly trade winds associated with the winter Asian monsoon. As boreal winter gives way to summer, the TRB migrates northwards (~10°N) and the wind direction reverses, blowing in a south-westerly direction, with the strongest winds, associated with the summer Asian monsoon ("*Somali Jet*"), prevailing over the Somali Peninsula. The seasonal migration of the TRB also gives rise to the East African monsoon, which results in northerly winds over northeast Ethiopia during boreal summer. The HoA also experiences regional to mesoscale convective phenomena, such as the breakdown of nocturnal Lower-Level Jets (LLJ), land-sea breezes and dust events generated by downdrafts from deep moist convective clouds also called haboob dust storm events, which can occur throughout the year but are most prevalent during boreal summer (S. D. Miller et al., 2008; Schepanski et al., 2009; Sutton, 1925).

Seasonal shifts in the position of the TRB drive seasonal changes in precipitation across the HoA. There are two rainy seasons: the "long rains" and the "short rains" (Figure 2a). The "long rains" occur in spring between March and May (Figure 2a), delivering around half of annual precipitation amounts (Billi, 2022a; Fazzini et al., 2015; Nicholson, 2017; Tierney et al., 2015). The "short rains," which occur between October and November, contribute less rainfall overall and are typically less reliable than the long rains (Nicholson, 2017). Average annual precipitation amounts across the study area show strong spatial variation (Figure 2b) (Billi, 2022a; Fazzini et al., 2015) with topography exerting a strong first order control (compare Figures 2 and 3). Very little rain falls over the low lying Afar and Danakil depressions, which are extremely dry, while the surrounding mountain ranges, especially the Ethiopian Highlands and the Ahmar Mountains, receive most of the precipitation that falls over the HoA (Figure 2b). Low average annual precipitation amounts (~400 mm/a) are observed across the Somali Peninsula, resulting in an arid to semi-arid climate with little vegetation cover. Even drier conditions prevail in the north of the Somali Peninsula, where average annual precipitation is less than 200 mm (Billi, 2022a; Fazzini et al., 2015) (Figure 2b). Precipitation predominantly occurs during two equinoctial wet periods associated with the shift of

the TRB (Liebmann et al., 2014) and there are two dry seasons, one during boreal summer and one during boreal winter (July to September and December to February, respectively) (Figure 2a).

Temperatures across the HoA are also strongly affected by topography (Figure 2c). The world's highest annual mean temperatures (~35°C) are recorded in the Afar and Danakil depressions with summer mean temperatures of 41°C (Billi, 2022a; Fazzini et al., 2015; Pedgley, 1967). Mean annual temperatures in Somalia are largely uniform across the entire country with an average of approximately 26°C. Progressively lower temperatures are recorded with increasing altitude in the Ethiopian Highlands and the Ahmar Mountains with average annual temperatures of 20°C at 1,500 m above sea level (m.a.s.l.) and with only a few days of frost recorded every year (Billi, 2022a; Fazzini et al., 2015).

Over the last 30 years, rainfall amounts have declined during the long rains season (Funk et al., 2008; Lyon & Dewitt, 2012; Williams & Funk, 2011) leading to an increased frequency of droughts (Anderson et al., 2022; Haile et al., 2019). As a result of this trend and the scarcity of arable land and its extreme vulnerability to erosion-induced soil degradation (Lal, 2014; Morton, 2007; Seife, 2021), the region has experienced several severe food security crises in recent decades (Krishnamurthy et al., 2020).

3. Methods

We present a new regional map of DSAF covering the HoA, developed using high-resolution satellite observations from the MSG SEVIRI instrument for a study interval spanning between 1 March 2006 and 28 February 2010 (see Data Availability Statement for data access).

3.1. Technical Specifications of Dust Retrieval From MSG-SEVIRI

Data from January 2004 onwards are available from the SEVIRI instrument onboard of the MSG through the European Organization for the Exploitation of Meteorological Satellites. MSG is a geostationary satellite orbiting at 0° above the equator that offers data of unmatched temporal (every 15 min) and spatial (3 × 3 km at nadir) resolution for the whole of the African continent and Southwest Asia.

It is challenging to detect airborne dust over desert surfaces using information from the visible (VIS) or infrared (IR) part of the wavelength spectrum solely, that is, using only one wavelength band (channel). This is because the spectral signatures of suspended dust are very similar to the signature of barren soil. In the VIS, the bright signature of a dust storm blurs with the desert background. In the IR, the brightness temperature (BT) of the dust plume and the surface may also be in a similar range. Therefore, to produce a dust source activation map, we used the SEVIRI "Dust RGB" product, which has been widely used to determine dust source locations across arid environments in North Africa (Ashpole & Washington, 2012; Schepanski et al., 2007, 2009) and southwest Asia (Hennen, 2017; Hennen et al., 2019). The Dust RGB product is generated using the brightness temperature differences (BTDs) and BTs of three thermal infrared wavelength bands centered at 8.7, 10.8, and 12.0 μm, where dust and aerosol display strong spectral variation and the atmosphere is nearly transparent (Ackerman, 1997; Schepanski et al., 2007; Sokolik, 2002). Each color channel (also called "color beam") of the Red, Green, Blue (RGB) composite image is assigned to a thermal wavelength band, which is the difference of two different thermal infrared wavelength bands, reflecting their BTs and BTDs. To distinguish airborne dust from thin clouds, the difference in BTs of the red channel (12.0–10.8 μm) is used. The red channel physically relates to optical thickness of dust and clouds, where dust aerosols display greater, thus positive, absorption at 10.8 μm than 12.0 μm, while thin cirrus clouds display the opposite (negative) absorption (Ackerman, 1997; Fuell et al., 2016). The green channel (10.8–8.7 μm) is used to differentiate between dust and the underlying desert surface, where desert surfaces have a lower emissivity at 8.7 μm than at 10.8 μm (large positive BTDs) while dust and clouds have a nearly equal emissivity over these wavelengths (small positive BTDs). To provide information about surface and cloud temperature, the BT of the blue channel is also included at 10.8 μm band. By combining the difference of BTs in red (12.0–10.8 μm) and green (10.8–8.7 μm) channels with the blue channel (10.8 μm), dust can be easily distinguished by its pink/magenta color from surrounding clouds and desert surfaces during day and night. In general, cirrus clouds are represented by black color, thick high-level cold clouds are dark red, thick mid-level clouds are yellow, thin mid-level cloud are green, hot sandy desert and dry air mass are bright blue, volcanic ash is orange/peach, humid air in lower levels are darker blue and cold air in lower levels are lilac (Banks et al., 2018, 2019). It is important to note that the dust RGB product is a composite image with single color that

represents a combination of different individual color intensities, therefore, the dust index may vary depending on thickness of the dust plume, underlying surface emissions and dust plume height in the atmosphere (Banks et al., 2018, 2019; Schepanski et al., 2007).

Every available image from the study region during the study interval (total of 1,461 days) was visually inspected to identify dust plumes across the study region. Observed individual dust plumes were backtracked through consecutive images to their starting location, which was determined by tracking each dust plume to the point of first appearance. The time of the first occurrence of each dust plume was then recorded as the time of dust source activation. For every dust plume observed, we also recorded cloud cover conditions at source location, that is, cloud free or clouded conditions. This allows us to infer the level of confidence and to investigate regional climatological conditions. In addition, because the HoA is located downwind from other dust producing regions (e.g., the Arabian Peninsula and northeast Africa), dust plumes that originated outside of the study region were also noted to examine the frequency of occurrence of dust plumes drifting into the study region.

3.2. Dust Activation Frequency Mapping

Our study interval spans between March 2006 and February 2010 and we report DSAF with a maximum frequency of one dust event per day per $1° \times 1°$ grid cell. This approach results in a weighting of the observed time-of-dust activation per grid cell toward the earlier activation. Observations show that more than once a day dust activation per grid cell seldom occurs across the study region, similar to observations in North Africa (Schepanski et al., 2009). Dust source activations obscured by clouds were not recorded. All data are presented as DSAF (in %) values following the method of Schepanski et al. (2007), and are calculated as follows:

$$\mathrm{DSAF}\,(\%) = (N_s / N_D) \times 100$$

$N_s = t$otal number of days containing one or more dust events in $1° \times 1°$ grid cell within a given interval,

$N_D =$ number of days of available satellite observation in the same interval

Seasonal DSAFs were defined as follows (a) spring (1 March to 31 May), (b) summer (1 June to 31 August), (c) autumn (1 September to 30 November), and (d) winter (1 December to 28/29 February).

3.3. ERA5

To compare our DSAF % observations to meteorological conditions, we used the European Centre for Medium-Range Weather Forecasts Reanalysis 5 (ECMWF ERA5) data set spanning the same 4-year time interval (March 2006–February 2010) as our satellite observations. The ERA5 data set is the fifth generation ECMWF reanalysis that uses model data with observations and is available from 1940 (Muñoz Sabater, 2019). We use ERA5-Land Monthly averaged data set by hour of day to analyze the summer average wind speed (using the 10 m u-component and v-component of wind in m/s), ERA5-Land Monthly aggregates of u and v surface wind component to infer seasonal distribution of average surface winds speeds and wind direction. We also use ERA5 hourly data on single levels (975 and 770 hPa) to analyze the difference in average early morning windspeeds. The ERA5 data sets have a relatively high resolution where ERA5-Land has a horizontal resolution of $0.1° \times 0.1°$ and ERA5 hourly data on pressure levels has a horizontal resolution of $0.25° \times 0.25°$. The ERA5 data sets offer a readily accessible, publicly available resource and the data are derived using a uniform methodology and model but we note some limitations. First, the ERA5 reanalysis data are generated based on assimilation of satellite observations, weather station data and other instruments which are used in the numerical weather model framework for a region where observational data are extremely sparce. Second, reanalysis data may differ from ground observations because of variability on small spatio-temporal scales and are also affected by local terrain and vegetation. Third, the ERA5 data sets are seasonally averaged over the 4-year study period in the entire HoA region. This process attenuates signal fluctuations, making it challenging to distinguish annual differences between each season and failing to capture localized wind speed peaks and significant regional events that could contribute to dust export.

4. Results and Discussion

4.1. Annual Dust-Activation Frequency in the Horn of Africa

Our multiannual DSAF map of the HoA shows one dominant dust active region and two secondary ones (Figure 3a). The Afar Triangle, bounded by the Ethiopian Highlands and the Ahmar Mountains and encompassing the Danakil

and Afar depressions (Figure 3b) is, by far, the most dust-active region in the HoA with a multiannual DSAF of 17.3%. The most important of the secondary dust producing regions is the Ogaden region in eastern Ethiopia and western Somalia where the Shebele and Ogaden river valleys are located (DSAF of 2.9%) (Figure 3). The other secondary region is the Nogal, featuring the Nogal Valley on the Somali Peninsula and the north-western tip of Somalia where multiannual DSAFs of up to 1.1% are recorded (Figure 3). A small number of dust events also occur within the Bogal-Bor region, named after two seasonal rivers in east Kenya, and the Guban basin, along the Gulf of Aden coastal plain, north of Ogaden (Figure 3). Dust storms originating from outside of the HoA study region are also recorded. During our study interval, 106 dust plumes drifted into our study region from elsewhere, with most occurring in the summer (82.1%). These imported drifting plumes were evenly distributed across the years, with 26 ± 1 events occurring each year between March 2006 and December 2009. These plumes move in a south to south-easterly direction toward the HoA, primarily originating from the Arabian Peninsula with a smaller proportion derived from the eastern Sahara.

In agreement with Prospero et al. (2002) and Ginoux et al. (2012) we identify the Danakil Depression as a major dust hot spot within the HoA (Figures 1a and 1b). However, we also identify an even higher frequency of dust events originating in the Afar Depression which was not previously identified as an important dust producing region. Ginoux et al. (2012) reported the Nogal Valley and a southeast coastal desert of Somalia as important dust producing regions. However, based on our multiannual DSAF %, we find that dust activation in these two areas is modest and non-existent, respectively, suggesting that many of the dust events reported by Ginoux et al. (2012) for these regions were not locally produced. These events may originate elsewhere in the HoA, but based on our observations, it is also possible that some of them originated on the Arabian Peninsula or in the eastern Sahara/Sahel. Our observations also call into question the reliability of the modeled reconstructions of Gherboudj et al. (2017). In direct contrast to those model-based reconstructions, we identify the Afar Triangle as the main dust hot spot on the HoA with the Somali Peninsula a minor contributor (Nogal Valley, Ogaden Desert and northern Somali coastal desert) (compare Figure 3a with Figure 1c).

4.2. Seasonality and Diurnal Frequency of Dust Activation in the Horn of Africa

Our data show strong seasonality in dust activation over the HoA (Figure 4, Figure S1). The dry summer season is the most dust-active time of year (Figure 4b and Figure S1), with maximum summer DSAF values of 31.9% recorded in the Afar Triangle. The Ogaden and Nogal regions are also predominantly active during the summer and record DSAF peaking at 9.5% and 4.1%, respectively. Similarly, in the Bogal-Bor and Guban regions, highest DSAF are recorded during the summer with peak DSAF of 3.0% and 2.5%, respectively. Overall, DSAF decreases into autumn and winter which are the least dust active times of the year before reawakening in spring and increasing in summer (Figures 4a–4h and Figure S1).

Our data also show that regional mean wind strength is a poor predictor of dust activation in the HoA (Figure 4). By far the strongest mean winds in the region blow from the southwest over the Somali Peninsula driven by the summer Asian monsoon (Figure 4j). Yet even at this time of the year, DSAF is much higher in the Afar Triangle where mean regional wind speeds are far lower (Figures 4j and 5). This result points to the control exerted on DSAF by (a) meteorological forcing at smaller spatial and shorter time scales and (b) spatial variability in availability of readily deflated surface material. The strong diurnal signal in our data (compare the top and middle panels in Figure 4) helps verify this interpretation.

Our data also show very strong diurnal variability in dust emission frequency with most activation events (82.1%) occurring between 08:00 and 16:00 and only 1.6% of events occurring between 20:00 and 06:00 (UTC + 3, local time of the study region; Figures 4 and 5). The Afar Triangle has two diurnal peaks in dust activation, the first occurring between 08:00 and 11:00 (UTC + 3) followed by a second between 13:00 and 16:00 (UTC + 3; Figures 4 and 5). Dust emissions from within the Ogaden and Nogal regions predominantly occur in the hours between 08:00 and 12:00 (UTC + 3). We attribute the morning peak in dust activation over the HoA, especially in the Afar Triangle and to some extent in the Ogaden, to the breakdown and downward shift of the LLJ with the onset of solar heating (Knippertz & Todd, 2012). Figure 5 shows the difference in wind speed (v-component) between two pressure levels in the atmosphere (975 and 770 hPa) at 06:00 (UTC + 3) during all four seasons. The data reveal that high dust activation during the morning hours, primarily in the summer in the Afar Triangle under clear-sky conditions, is driven by the breakdown of the LLJ, which is expressed by large differences in average early morning windspeeds (Δv_{mean}) (Figures 5b–5e). The LLJ can be observed in all subtropical desert regions, developing in dry, cloud-free conditions when intensification of surface insolation creates a hot and deep convection boundary layer (CBL) (Knippertz & Todd, 2012). At night, temperatures above the land surface cool,

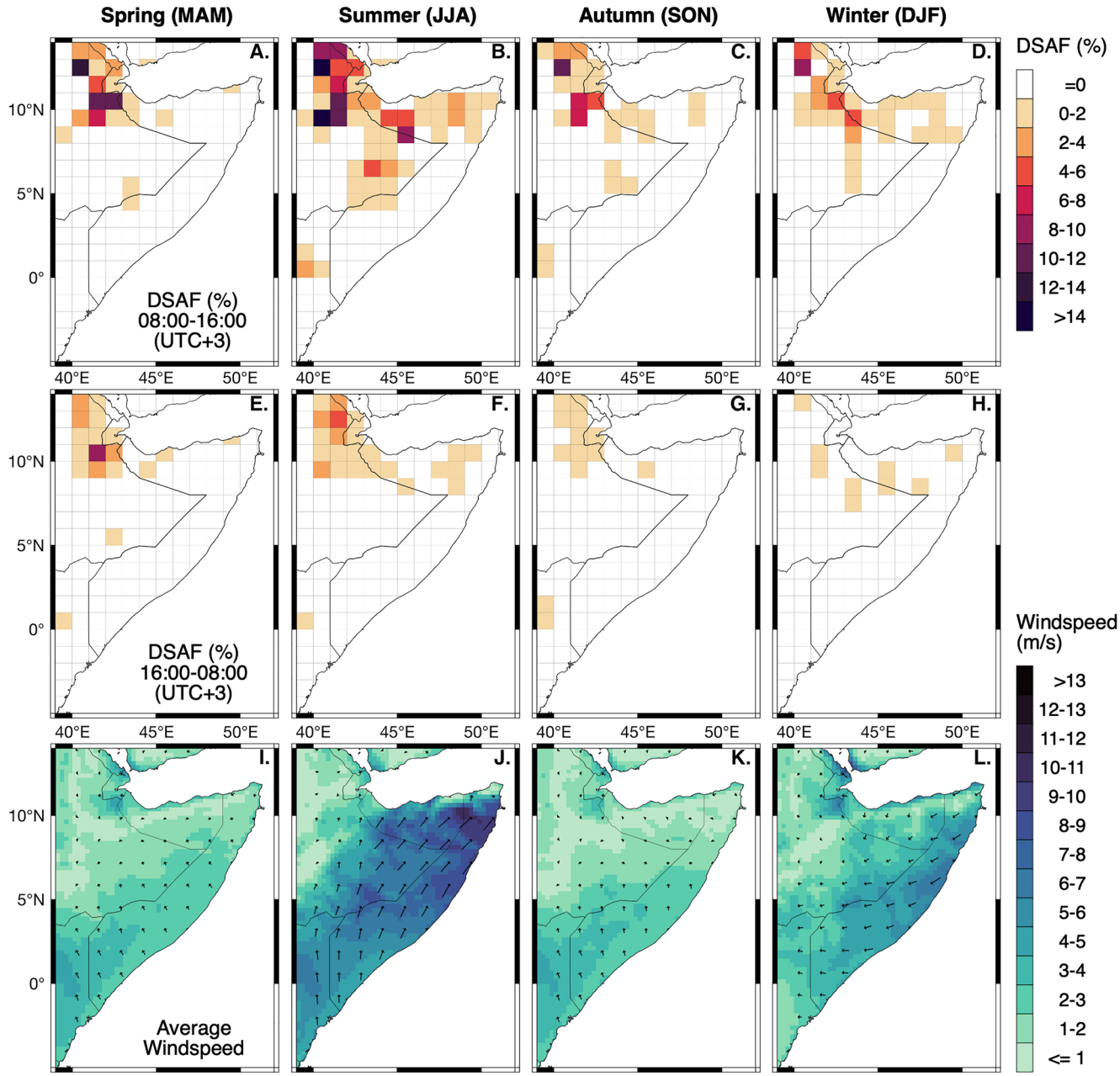

Figure 4. Seasonal and diurnal dust activation compared to regional mean windspeed. Top panel shows dust source activation frequency (DSAF) (%) for daytime hours (08:00–16:00, UTC + 3; local time); middle panel shows DSAF (%) for night-time hours (16:00–08:00, UTC + 3; local time); bottom panel shows wind strength (color and arrow length) and direction (arrow direction). Seasons labeled by column. Seasonal distribution of average surface winds speeds and wind direction vectors (i–l) between March 2006 and February 2010 from ERA5 Monthly Aggregates (*u* and *v* surface wind component; from Google Earth Engine (GEE)) (Muñoz Sabater, 2019).

creating a strong temperature inversion between the CBL and the land surface which results in a separation of these two layers. As the solar heating increases during sunrise, the vertical decoupling of the atmosphere begins to erode, creating turbulence and strong surface winds (Fiedler et al., 2013; Schepanski et al., 2009; Washington et al., 2006). While in Figures 5b–5e, we only show the difference between two pressure levels at 06:00 (UTC + 3) when the difference is generally greatest, this phenomena drives strong surface winds and particularly active dust emissions from early morning to midday (Knippertz & Todd, 2012; Schepanski et al., 2013) and has also been documented in the Sahara and the Arabian Peninsula (Hennen, 2017; Schepanski et al., 2012).

The second peak in diurnal dust activation occurs in the afternoon, between 13:00 and 16:00 (UTC + 3) and can be attributed to increased haboob activity (S. D. Miller et al., 2008; Schepanski et al., 2009, 2017), primarily in

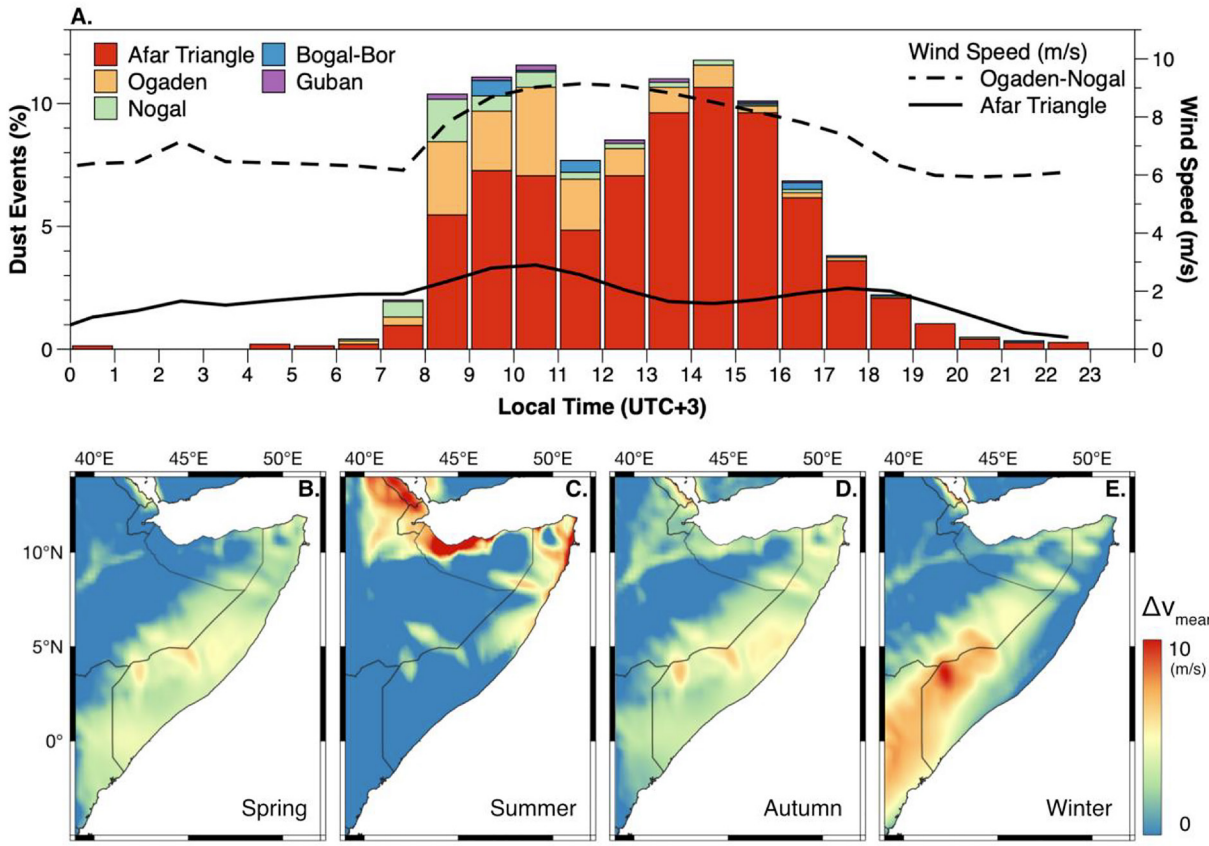

Figure 5. Diurnal variability in dust activation over the Horn of Africa and indicators of its mechanistic forcing. (a) Diurnal variability of dust activation expressed in number of dust events (colored bars, %) compared with average wind speed (black lines, m/s) during the summer season (JJA). The number of dust events (%) is calculated from the total number of dust events recorded within the study region with the Afar Triangle shown in red, Ogaden in pale orange, Nogal in green, Bogal-Bor in blue, and Guban in purple. Summer (JJA) average wind speed (m/s) is extracted from *u* and *v* wind component at 10 m during the study interval between March 2006 and February 2010 from ERA5-Land Monthly Averaged by Hour of Day (from Google Earth Engine (GEE), Muñoz Sabater, 2019). Summer wind speeds were selected as around half of all dust events occur during the summer seasons. (b–e) Difference between average early morning windspeeds (Δv_{mean}) between two pressure levels (975 and 770 hPa at 06:00 UTC + 3), as an indication of the breakdown of the Lower-Level Jets in (b) spring, (c) summer, (d) autumn, and (e) winter. Calculated from ERA5 hourly data on single levels using seasonal mean of *v*-component wind speed (from GEE, Muñoz Sabater, 2019).

the Afar Triangle (see Section 4.3.1 for details). While our DSAF data set does not provide a quantitative index of atmospheric dust load, it is the first available remote sensing data set to offer insight into the diurnal variability of dust emissions which allows an estimation on the synoptic and mesoscale conditions that are the likely forcing mechanism of dust activation.

4.3. Dust Activation in the Horn of Africa by Region

Dust deflation requires favorable climatic and land surface conditions including strong surface winds, strong vertical velocities and low soil moisture, providing readily deflatable sediment (Webb & Strong, 2011).

4.3.1. On Dust Activation in the Afar Triangle

By far the most dust-active region in the HoA is the Afar Triangle, accounting for 77.1% of all observed events in our study. In fact, 36.1% of the dust events documented in our study occur in the Afar Triangle region in summer alone (Figure 4b). Our data show that 92.5% of dust events in the Afar Triangle occur between 08:00 and 18:00 (UTC + 3) and, while these occur under both clear sky and clouded conditions in the afternoon hours, there is a strong tendency for dust activation under clear skies in the morning hours (Figure 6). The summer southwest monsoon does not exert a major influence on the Afar Triangle (Figure 4); thus we attribute dust activation here to some combination of (a) sea breezes from the Red Sea, (b) breakdown of the LLJ, and (c) haboob dust storm events. The first two of these mechanisms lead to dust-producing events throughout the day and are associated with clear sky conditions, while haboobs develop primarily during the afternoon hours under clouded skies.

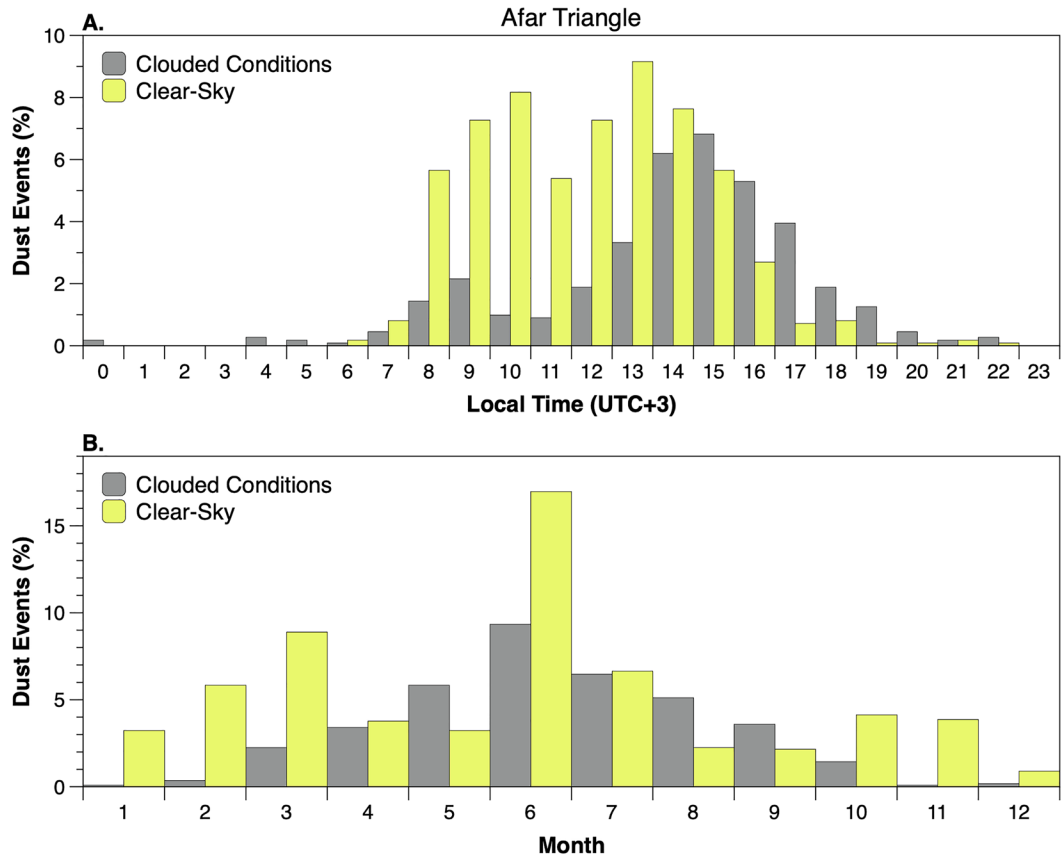

Figure 6. (a) Diurnal and (b) seasonal distributions of dust activation (% of all events) from within the Afar Triangle under clouded (gray) versus clear-sky (yellow) conditions. Dust activation under clear sky conditions prevails throughout the day between 08:00 and 16:00 (UTC + 3) while dust activation under clouded conditions predominantly occurs in the afternoon hours between 14:00 and 18:00 (UTC + 3). While breakdown of the Lower-Level Jets and land-sea breezes occur under clear-sky conditions primarily during the morning hours and throughout the day, respectively, the haboob dust storm events mostly occur in the afternoon hours under clouded conditions associated with a moist convection process. Seasonal distribution of dust activation shows increase in dust events under clear sky condition primarily during June. Dust activation under clouded conditions also largely occurs during the summer months.

Of all the dust events that occur under clear-sky conditions, just over half (53.9%) occur before 12:00 (UTC + 3; Figure 6a). The influence of sea breezes on dust activation is strongest near the coast in the daytime hours, during which a large pressure gradient develops due to the differential heating between land and sea (S. T. K. Miller et al., 2003). Red Sea land-sea breeze circulation is one of the strongest in the world, extending up to 200 km inland and occurring almost daily throughout the year with a peak in the summer season (Davis et al., 2019; Khan et al., 2018). The largely morning occurrence of LLJ breakdown and day-time occurrence of land-sea breeze circulation coincides with an increase in dust emissivity in the Afar Triangle suggesting that both phenomena play a role in deflation events in the HoA's most dust-active region.

Of all the dust-producing events observed in the Afar Triangle, 38.2% of them occurred under clouded sky conditions with most of these (82.6%) occurring after 12:00 (UTC + 3; Figure 6a) and during summer months (54.8%; Figure 6b). These events are mainly driven by the formation of moist convection processes triggering haboob dust storms, which entrain large amounts of sediment that can be transported for hundreds of kilometers (Knippertz et al., 2007; Sutton, 1925). Haboobs form predominantly during spring and summer months (Sutton, 1925), when strong solar insolation is accompanied by a rise in relative humidity fostering deep moist convection. Similar forcing is observed in the Sahara and the Arabian Peninsula where moist air is transported over dry land surfaces that are directly overlain by a hot surface air layer (Knippertz & Todd, 2012; S. D. Miller et al., 2008; Schepanski et al., 2009; Sutton, 1925). This results in the formation of mesoscale convective systems driving strong downdrafts of cold air, creating a turbulent flow as they converge with warm surface air (S. D. Miller et al., 2008; Sutton, 1925). These events commonly occur in late afternoon as a result of the diurnal cycle of moisture convection (S. D. Miller et al., 2008)

and interaction with nearby orographic features, when warm air rises, cools and condenses resulting in a formation of convective cloud along the mountain range and a strong air turbulence driving dust activation (Knippertz et al., 2007; Mekonnen & Rossow, 2018; S. D. Miller et al., 2008). In the Afar Triangle, haboobs are formed when moist air transported from the Red Sea and the Indian Ocean over-rides hot, dry surface air over the baking hot lowland basins (e.g., Mekonnen & Rossow, 2018; Viste & Sorteberg, 2013). The occurrence of haboobs within this region is also stimulated by the high relief along the western and southern borders of the Danakil and Afar depressions, that is, the Ethiopian Highlands and the Ahmar Mountains (Figure 3b; Mekonnen & Rossow, 2018). Haboob-induced dust emissions are often underrepresented in global emission models (Knippertz & Todd, 2012). This study does not provide a full record of haboob-related dust activation because more detailed information on cloud type and local change in humidity are needed but our use of a sub-hourly data set represents an important step in this direction.

Favorable land surface conditions also contribute to high dust emissions from the Afar Triangle. The region is located at the northern end of the Great Rift Valley. Geologically, it is mostly composed of magmatic and pyroclastic materials in a form of flows, domes, ignimbrites, tuffs and scoria cones (Beyene & Abdelsalam, 2005; Varet, 2018). The volcanic formations are overlain by a host of different types of Cenozoic sedimentary basins (Billi, 2015). Axial and peripheral basins occur along the margins of the Afar Depression at the foot of western and southern escarpment along the Awash River. Sedimentary deposits in these basins can be up to 1,000 m thick, comprising fluvio-lacustrine sediments including shales, sands, pebbles and carbonate deposits interspersed with ash deposits and basalt flows (Billi, 2015; Varet, 2018). The Awash River is an important source of fluvial sediment to the Rift Valley. It is the second longest river in Ethiopia with a catchment area about 110,000 km^2 (Tola & Shetty, 2021). It transports material from the Ethiopian Highlands where it originates, through the Rift Valley to the lowland plain of the Afar Depression where it terminates in Abe Lake (Billi, 2015). The main tributaries to the Awash River are mostly small and come from the west, while on the eastern margin of the rift escarpment north of the Ahmar Mountains, tributaries are ephermal and often do not reach the Awash River. Rivers in the Danakil Depression are all ephermal and most show a downstream decrease in discharge and terminal fan on the floor of the basin. Very few of these rivers even drain into the small/ephemeral hypersaline hydrothermal spring-fed lakes in the region such as the Afrera and Asale lakes and none of them reach the Red Sea (Billi, 2015). The arid conditions which stem from the low annual precipitation rates and high temperatures (Figure 2) in this extremely low lying region (Figure 3) combined with large volumes of readily deflated fine fluvial sediment delivered by the lower reaches of the Awash River or exposed by post-African Humid Period desiccation of water bodies (Gasse, 1974) and limited vegetation cover create the ideal surface conditions for dust activation.

4.3.2. On Dust Activation in the Ogaden and Nogal Regions

In the Ogaden and Nogal regions, the main driving mechanism for dust export during summer is the intensification of the southwest monsoon winds, which reach an average of more than 14 m/s in the summer (Figure 4j). Overall, vegetation cover in the HoA is greatest at high elevations, for example, the Ahmar Mountains north of Ogaden and Nogal regions, where precipitation amounts are highest (Figure 2b) but vegetation cover is sparse in the arid lowland regions of Ogaden and Nogal Valley (Billi, 2015). This leaves bare surface land area exposed and vulnerable to wind and river erosion (Fenta et al., 2020). However, here dust activity is modest even during summer when strong southwesterly monsoon winds sweep across the Somali Peninsula (Figure 4). This result is presumably attributed to a paucity of loose, readily deflated fine sediment on the land surface possibly driven by long intervals without rainfall-driven erosion to produce fresh unconsolidated material leaving stony desert pavement surfaces, which are devoid of fine, readily deflatable material (Mège et al., 2015; Merla et al., 1973; Parajuli & Zender, 2017) (see Section 4.4 for more details).

4.4. Interannual Variability of Dust Activation in the Horn of Africa

Higher DSAFs are recorded in 2008 and 2009 compared to the interval between March 2006 and December 2007 (Table 1). Of all recorded dust events in our study, 40.6% take place in 2009 and 28.7% in 2008 compared to only 13.6% in 2007 with the reminder occurring during partial study years (2006 from the start of March and 2010 to the end of February, 12.1% and 5%, respectively). In the Afar Triangle, the proportion of dust events approximately doubles from 2007 to 2008 and 2009 while the jump in the Ogaden region on the Somali Peninsula is even larger–by a factor of three from 2007 to 2008 and a factor of nearly 10 from 2007 to 2009 (Table 1, Figure 7).

We attribute the increase in dust events from 2007 to 2008 and from 2008 to 2009 to elevated rainfall amounts during the early portion of our study interval followed by low rainfall amounts and reduced vegetation cover in

Table 1
Interannual Variability of the Total Number of Dust Events (%) for Each Region: Afar Triangle, Ogaden, Nogal, Bogal-Bor, and Guban

	Afar Triangle (%)	Ogaden (%)	Nogal (%)	Bogal-Bor (%)	Guban (%)	Total (%)
2006 (from March)	*9.6*	*0.9*	*0.2*	*1.3*	*0.1*	***12.1***
2007	12.9	0.5	0.2	0.0	0.0	**13.6**
2008	23.5	3.1	1.3	0.1	0.7	**28.7**
2009	27.5	9.6	3.0	0.3	0.2	**40.6**
2010 (until March)	*3.6*	*1.3*	*0.1*	*0.0*	*0.0*	***5.0***
Regional Total (%)	**77.1**	**15.4**	**4.8**	**1.7**	**1.0**	**100**

Note. 2006 and 2010 records do not include dust source activation frequencies for the entire year, 2006 record starts in March and 2010 ends on the 28 February. The bold values indicate the total % and the italics values indicate the years that are not complete.

2008 and 2009 (Figures 7 and 8). Based on the 40-year average Climate Hazards Group InfraRed Precipitation with Station precipitation pentad data, annual precipitation amounts in our study region were above average in 2006 (+24.8%) and 2007 (+1.4%) whereas they were below average (−12.4% and −14.1%) in 2008 and 2009, respectively (from GEE; Figures 8e–8h). Based on the 40-year precipitation record, highest total precipitation in the HoA was recorded in 1997 (+63.3%) and lowest in 1984 (−25.2%) with the years 2006 and 2007 being the 4th and 13th wettest years on record and years 2008 and 2009 being the 4th and 9th driest, respectively.

Our study interval is too short to detect statistically meaningful interannual variability in our data but it is useful to consider our results in the context of the contemporaneous record of El Niño–Southern Oscillation (ENSO) and Indian Ocean Dipole (IOD) indices (Figure 7) because both of these modes of climate variability are suggested to influence the hydroclimate of the HoA (Abram, Hargreaves, et al., 2020; Abram, Wright, et al., 2020; Hafez, 2016; Mpelasoka et al., 2018). We record the highest DSAF during the summer of 2009 on the approach to the strong El Niño and positive IOD of that year (Figure 7). Complex interactions between ENSO and the IOD (Figures 7a and 7b) as well as the Inter-decadal Pacific Oscillation (IPO) and the North Atlantic Oscillation (NAO) makes drought prediction for the HoA far from straightforward. Many studies suggest that ENSO is the main cause of drought occurrence in the HoA (Hafez, 2016 and references therein), others suggest that overall climate variability within the HoA is more complex and most likely depends on the contemporaneous modes of the major climate variability drivers (i.e., ENSO, IOD, IPO, and NAO) (Abram, Hargreaves, et al., 2020; Behera et al., 2006; Kajtar et al., 2017; Mpelasoka et al., 2018). A positive IOD occurs when the Dipole Mode Index (DMI), the difference in sea surface temperature anomalies between the western equatorial Indian Ocean (10°S–10°N, 50°–70°E) and the south-eastern Indian Ocean (10°–0°S, 90°–110°E) (Saji et al., 1999), is more than +0.4°C, and has been linked to wetter conditions over the HoA (Abram, Hargreaves, et al., 2020). Few studies consider the spatial variations in rainfall resulting from the interactions of ENSO, IOD, IPO, and NAO, which can either enhance or supress the effect of these climate drivers and can alter their strength, periodicity and seasonality (Mpelasoka et al., 2018 and references therein). While dust activation increased from 2008 through 2009 compared to dust activation between March 2006 and end of 2007, neither ENSO or IOD are in their extreme phases between March 2008 and 2009 (Figure 7). However, preceding March 2008, the DMI index shows a positive IOD event (second half of 2006), which led to increased rainfall over the HoA, followed by strong La Niña (September 2007–March 2008), which led to reduced rainfall over the HoA (Figure 7), consistent with observations of precipitation trends during strong ENSO and IOD events (Abram, Hargreaves, et al., 2020; Hafez, 2016; Nicholson, 2017). Drought in the HoA from 2008 onwards, therefore, is most likely traced to the interaction of multiple ocean-atmosphere climate drivers.

The Ogaden and Nogal drainage basins have no major active rivers but are lined with seasonal "wadis" and palaeo channels (Abbate et al., 1993; Mège et al., 2015). The wadis are dry most of the time but they are reactivated during rainy seasons, especially by episodes of short and heavy rainfall, which often causes severe flooding that can last from hours to days (Bauduin et al., 1973). These intense episodic flooding events transport large volumes of surface sediments from the upper reaches of the catchment to the lowlands downstream where they are deposited (Bauduin et al., 1973). Thus, the above average rainfall amounts in 2006 and 2007, especially in high relief areas, such as the Ahmar Mountains (Figure 8) reactivated seasonal wadis and caused severe flooding in Ogaden and Nogal regions (FEWS NET, 2007) and likely fed the floodplains of the Ogaden and Nogal with

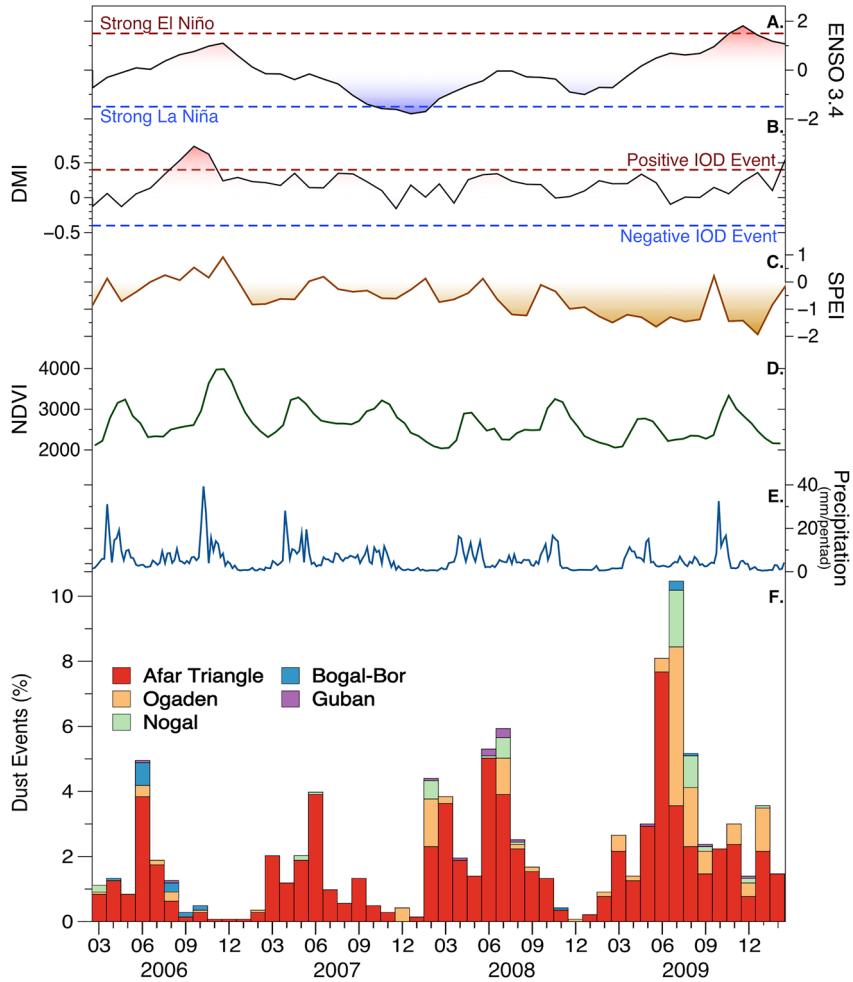

Figure 7. Interannual variability in dust activation in the Horn of Africa (HoA) from March 2006 to February 2010 compared to regional climatic conditions and global atmosphere-ocean phenomena. (a) El Niño–Southern Oscillation 3.4 index (Rayner et al., 2003), (b) Dipole Mode Index showing the Indian Ocean Dipole strength (Saji & Yamagata, 2003), (c) Standardized Precipitation-Evapotranspiration Index for the HoA (SPEI, Beguería et al., 2014) with negative values representing drought conditions, (d) Mean Normalized Difference Vegetation Index across the HoA from Moderate Resolution Imaging Spectroradiometer Terra 16-Day Global 250 m (from Google Earth Engine (GEE), Didan, 2015), (e) Climate Hazards Group InfraRed Precipitation with Station (CHIRPS) mean pentad precipitation rates from the HoA (mm/pentad, from GEE) (Funk et al., 2015), and (f) Proportion of total dust events (%) in: Afar Triangle (red), Ogaden (pale orange), Nogal (green), Bogal-Bor (blue), and Guban (purple) regions.

fresh fine-grained sediments (a common occurrence in northern Somalia, where material is deposited in a form of thin mud drapes, Billi, 2022b). Availability of flood deposits probably helps to explain the increase in DSAF during 2008 and 2009 (Figures 7 and 8) for two reasons. First, freshly dried out readily deflated unconsolidated fluvial and lacustrine sediments act to turbocharge atmospheric dust loading (e.g., Crocker et al., 2022 and references therein) and second, rainfed agriculture is prevalent in the Ogaden-Nogal region (Biswas et al., 1987) and concentrated in close vicinity to seasonal "wadis" (Buchhorn et al., 2020). Therefore, it is likely that natural and agricultural processes combine to explain the observed spike in DSAF in this region in 2008 and 2009.

4.5. Dust Activation: The Horn of Africa in the Regional Context

We combine our new data for the HoA with equivalent data for both North Africa from Schepanski et al. (2009) and the Arabian Peninsula through southwest Asia from Hennen (2017) as normalized by Kunkelova et al. (2022) to present an integrated map of annual DSAF % for the wider region (Figure 9). Our map reveals a striking latitudinal anomaly in dust activation. Modern day dust activation over North Africa and the Arabian Peninsula

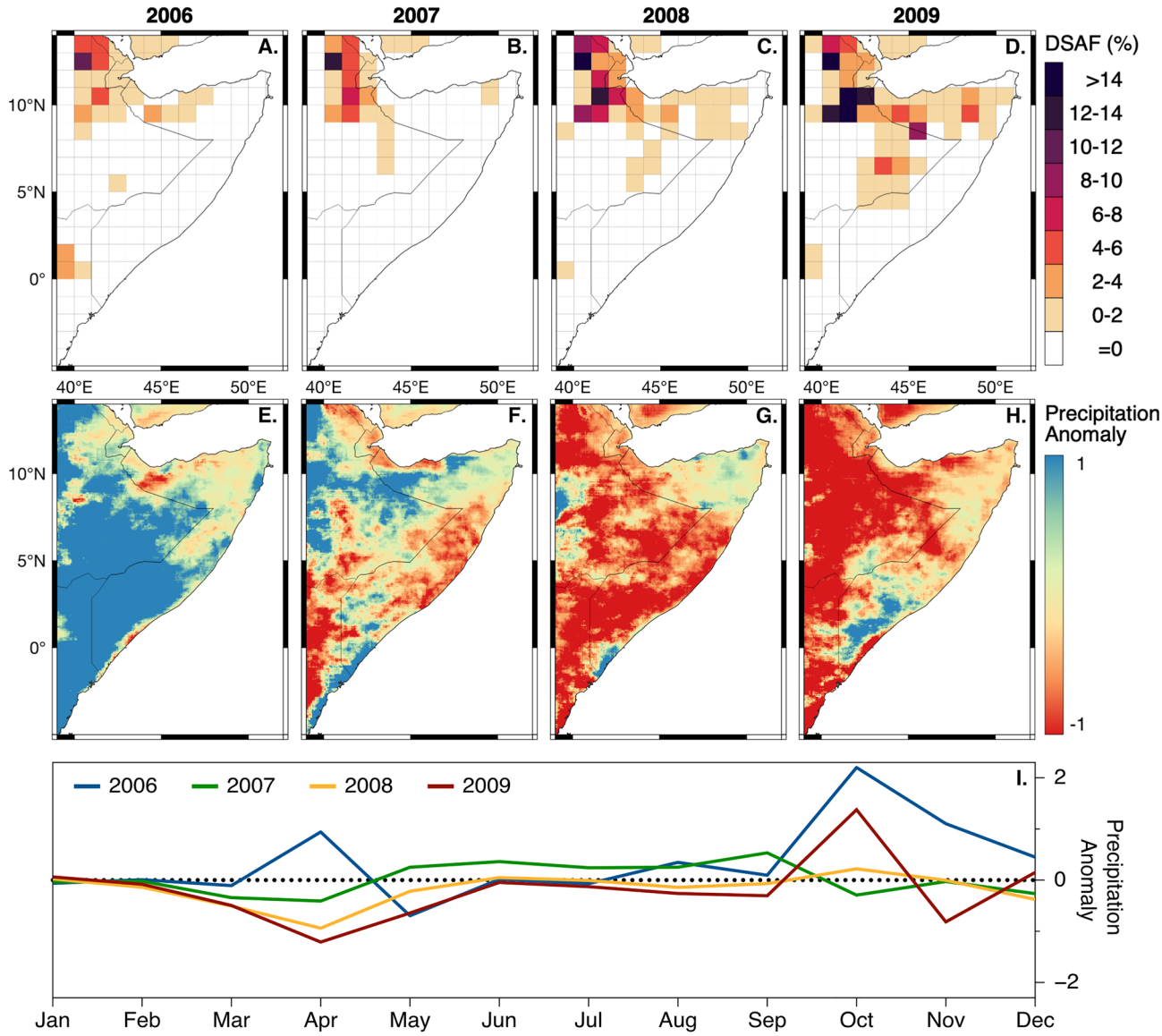

Figure 8. Dust activation (%) maps for (a) 2006 (from March onwards), (b) 2007, (c) 2008, and (d) 2009, compared with maps of annual precipitation anomalies (e–h) from 40-year average values (January 1981 to December 2020) calculated using Climate Hazards Group InfraRed Precipitation with Station pentad data (from Google Earth Engine (GEE), Funk et al., 2015). (i) Monthly change in precipitation anomalies across the Horn of Africa for the years of 2006 (blue), 2007 (green), 2008 (yellow), and 2009 (red) (from GEE).

is confined to latitudes north of ~13°N but it extends much further south in the HoA, deep into the equatorial belt. This result is rooted in the unusually arid climate conditions in the HoA considering its low latitude setting. This aridity stems from factors that include (a) the northward intrusion of the southern hemisphere subtropical high-pressure belt associated with northward migration of the TRB, (b) funneling of moisture transport into Central Africa by the valleys of the East African Rift System, (c) the Ethiopian Highlands acting as a rain shadow, and (d) cold oceanic currents from coastal upwelling along the Somali Peninsula reducing the supply of moisture to the region (Hession & Moore, 2011; Munday et al., 2023; Nicholson, 1996, 2017; Van den Hende et al., 2021). However, aridity alone is not a good predictor of dust activity. The dominant role played by the Afar Triangle in the HoA attests to the strong control exerted on dust activation by the availability of readily deflated unconsolidated sediments associated with ephemeral fluvial and lacustrine systems in low lying endorheic basins (Figure 9). In the case of the HoA, the lower Awash River is clearly very important in this regard (Figure 9).

A comparison between our new data for the HoA and equivalent published data for North Africa and Westernmost Asia broken down by the preferential dust source areas of Jewell et al. (2021) and Kunkelova et al. (2022), respectively,

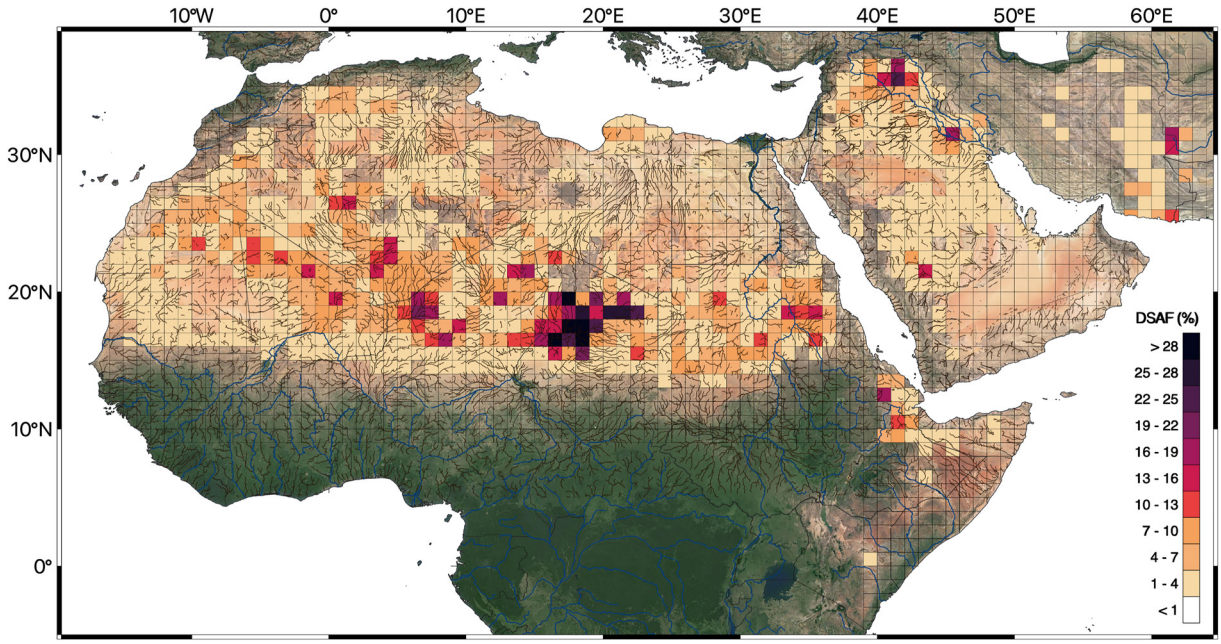

Figure 9. Integrated map of dust source activation frequency (DSAF, %) for North Africa (Schepanski et al., 2012), the Arabian Peninsula (Hennen, 2017), and southwest Asia (Hennen, 2017) and the Horn of Africa (HoA) (this study) for March 2006 to February 2010. Active rivers (blue lines) and palaeo-river reconstruction (brown lines) are also shown (Breeze et al., 2015; Manning et al., 2023). Palaeo-rivers reconstruction extends from 5° to 40°N covering all of North Africa, most of HoA and the Arabian Peninsula, excluding Iran. Highest DSAF (%) are commonly recorded in basins with desiccated or ephemeral water bodies, such as Megalake Chad in central North Africa, the Sistan Basin in east Iran and the Afar Triangle in the HoA as well as arid regions and flood plains surrounding active rivers, such as the Nile in the Nubian Desert of Sudan and the Euphrates and Tigris rivers in Mesopotamia. DSAF (%) data from Hennen (2017) are normalized to match the data resolutions of Schepanski et al. (2012) and this study. For detailed description on the method used for data normalization see Kunkelova et al. (2022).

reveals that dust activation in the HoA is unusually seasonal. Here, about ~40% of all annual events occur in June and July alone and this figure rises to over 50% if August is included (Figure 10). To a first order, this result is explained by the arrival of the dry season at the end of the "long rains" (typically end of May) which normally lasts until the start of the "short rains" in October (Figure 2). However, we must also consider the role of deflating winds. June through August are characterized by strong southwest summer monsoon winds that sweep across the Somali Peninsula but DSAF in the HoA is dominated by the Afar Triangle which lies beyond their influence (Figures 3 and 4). There, smaller scale meteorological events drive dust activation (see Section 4.2) and our analysis suggests that breakdown of the LLJ, land-sea breezes and afternoon haboobs in the Afar Triangle play an important role in driving the anomalously strong seasonal signal (summer spike) in dust activation in the HoA (Figures 6 and 10).

Diurnal variability in dust activation in the HoA is also distinct from the signal observed in North Africa where 95.3% of events occur before 12:00 local time throughout the study interval (March 2006–February 2010) (Figure 11a). In contrast, 64.4% occur before 12:00 local time in the Westernmost Asia and only 43.6% in the HoA (Figure 11b). The morning dust activation in Western, Central and Eastern N Africa regions is primarily attributed to breakdown of nocturnal LLJ (Schepanski et al., 2009), similar to interpretations of hourly data from Westernmost Asia (Hennen, 2017) and the HoA. While certain regions in Central N Africa, such as Akhdar area located in northeast Libya, may experience over 50% of dust activation between 12:00 and 00:00 UTC (Schepanski et al., 2012), overall afternoon activation in the North Africa is less frequent compared to the Westernmost Asia and the HoA. Afternoon activation in all regions is likely attributed to deep moist convection associated with the formation of haboob dust storm events (Schepanski et al., 2009). Based on the comparison of hourly distribution of dust activation, Westernmost Asia and the HoA experiences more haboob-driven dust events compared to all three sub-regions of the North Africa.

5. Conclusions

We present a record of DSAF for the HoA using MSG-SEVIRI dust index image over a 4-year period between March 2006 and February 2010. Our composite DSAF map for the wider region shows that the HoA is

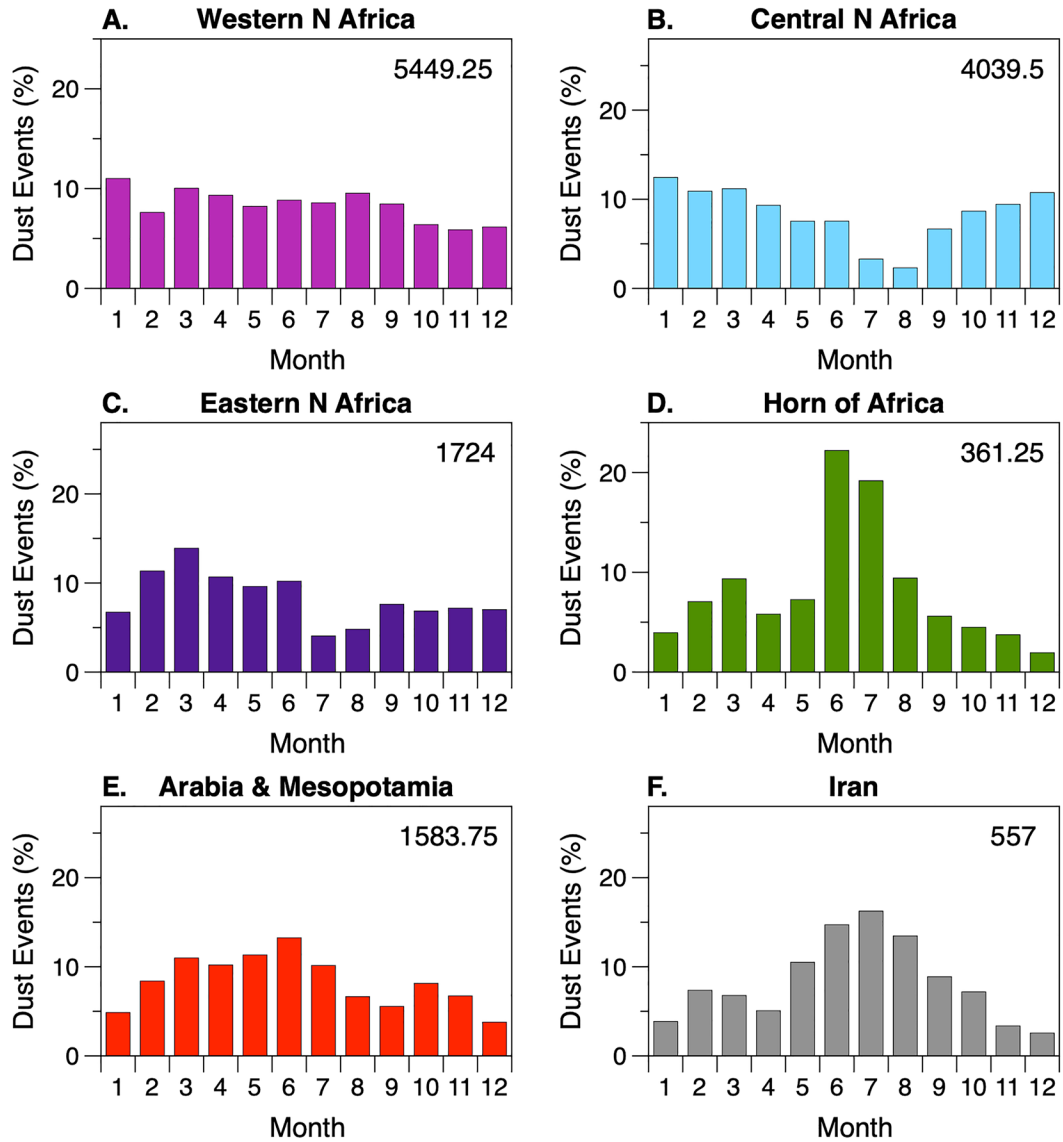

Figure 10. Seasonality of dust events (%) in (a) Western, (b) Central, and (c) Eastern North Africa (Schepanski et al., 2012); (d) Horn of Africa (this study); (e) Arabian Peninsula, and (f) Iran (Hennen, 2017). Dust events are represented as values in % to allow for a direct comparison. The number in the top right of each panel is the mean number of dust events per year recorded in that subregion. Month 1 is January.

latitudinally anomalous in being a dust active region that extends into the core of the tropics. The Afar Triangle, which encompasses the Danakil and Afar depressions, is by far the most dust active region in the HoA, accounting for more than 77% of all recorded dust events. The Afar Triangle is a dust activation hot spot because, situated at the northern end of the African Rift Valley, it is a hyper arid, low-lying endoreic basin fed by the lower Awash River system which gives rise to ephermal lakes and deep sedimentary basins containing readily deflated fine-grained sediments along the foothills of the Ethiopian Highlands and the Ahmar Mountains. Dust deflation and entrainment under clear sky conditions is primarily driven by the breakdown of low-level jets and land-sea breezes during the morning and daytime hours and by the formation of moist convection which triggers haboob dust storm events predominantly in the afternoon hours under clouded conditions. Our multiannual record shows that just over half of all observed dust events occur in summer, making the HoA an unusually seasonal source of dust to the atmosphere. Our results also show strong variability in dust activation throughout the day with the majority (>82%) of events occurring between 08:00 and 16:00 (UTC + 3). This result is similar to the diurnal signal documented in Westernmost Asia

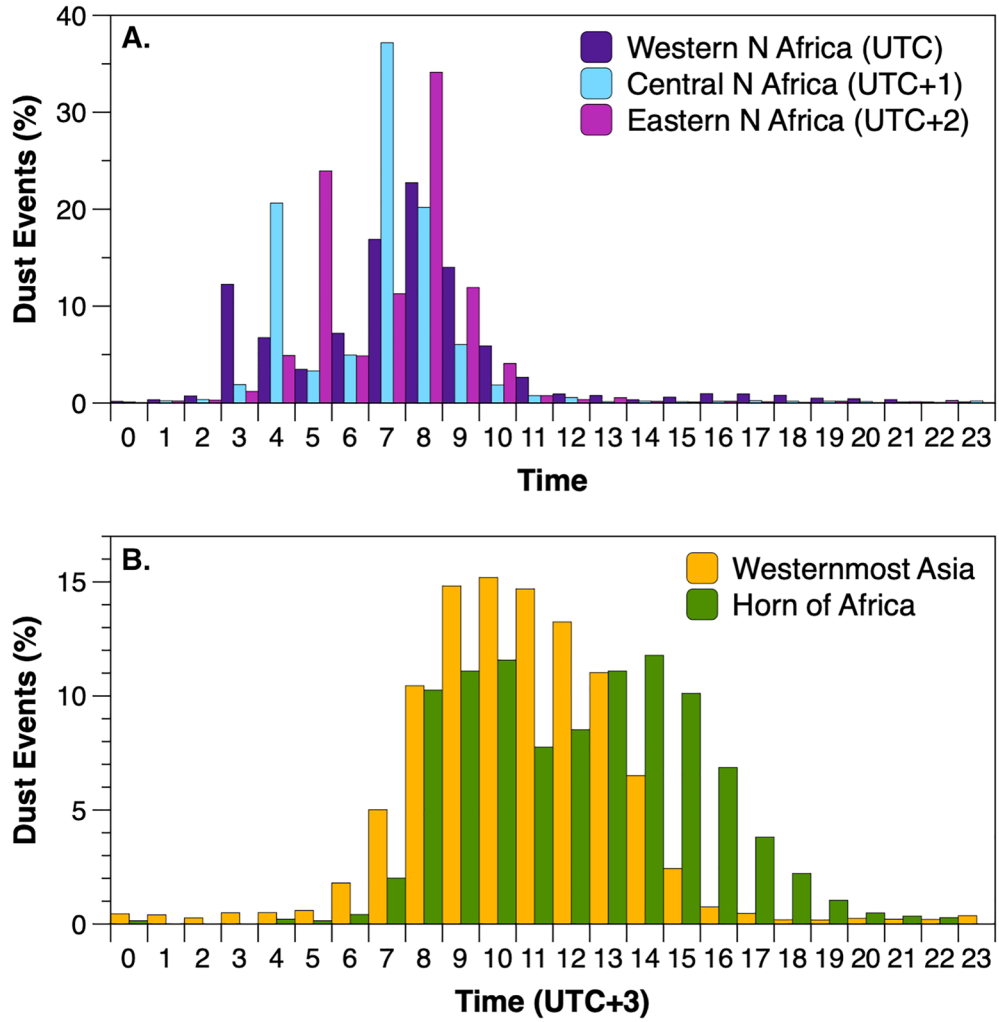

Figure 11. Comparison of diurnal distribution of dust activation between (a). North African dust producing regions (Western, Central, and Eastern) (Schepanski et al., 2009) and (b) Westernmost Asia (Hennen, 2017) with the Horn of Africa. The diurnal distribution is calculated from number of dust events occurring between March 2006 and February 2010 for all sub-regions. Each region is plotted to show local time. Note the different vertical scales in panels (a) and (b).

but the HoA is much more dust active in the afternoon hours than the North Africa. Dust events are also recorded in the arid to semi-arid Ogaden and Nogal valleys, located on the Somali Peninsula, but, despite strong prevailing summer southwest monsoon winds, these are modest in frequency in comparison to those of the Afar Triangle.

Seasonal changes in synoptic scale wind patterns and the associated changes in moisture transport control dust activation across North Africa, Westernmost Asia as well as the HoA. The most significant meteorological phenomena triggering dust events are nocturnal breakdowns of the LLJ, which are observed across all of these arid regions. Haboobs appear to be more prevalent in Westernmost Asia and the HoA than in North Africa.

Data Availability Statement

Data set for this research is available at the University of Southampton Institutional Research Repository (https://doi.org/10.5258/SOTON/D2874). Data previously published in the literature included in this paper include Kunkelova et al. (2022) (data available at https://doi.org/10.5258/SOTON/D2873) and Schepanski et al. (2012) (data available at https://zenodo.org/records/4072879).

Acknowledgments
We thank Jan El Kassar and Nicole Docter for their help with accessing the remote sensing data and stimulating discussions. This work was supported by the Natural Environment Research Council (NERC) (Studentship number NE/L002531/1 to TK) and Royal Society Challenge Grant CHG\R1\170054 (P.A.W.) and Wolfson Merit Award WM140011 (P.A.W.). Additional funding came from University of Southampton's GCRF strategic development fund Grant 519016 (P.A.W. and A.J.C.).

References

Abbate, E., Sagri, M., & Sassi, F. P. (1993). *Geology and mineral resources of Somalia and surrounding regions*. Istituto Agronomico Per L'Otremare.

Abram, N. J., Hargreaves, J. A., Wright, N. M., Thirumalai, K., Ummenhofer, C. C., & England, M. H. (2020). Palaeoclimate perspectives on the Indian Ocean Dipole. *Quaternary Science Reviews*, *237*, 106302. https://doi.org/10.1016/j.quascirev.2020.106302

Abram, N. J., Wright, N. M., Ellis, B., Dixon, B. C., Wurtzel, J. B., England, M. H., et al. (2020). Coupling of Indo-Pacific climate variability over the last millennium. *Nature*, *579*(7799), 385–392. https://doi.org/10.1038/s41586-020-2084-4

Ackerman, S. A. (1997). Remote sensing aerosols using satellite infrared observations. *Journal of Geophysical Research*, *102*(D14), 17069–17079. https://doi.org/10.1029/96jd03066

Alizadeh-Choobari, O., Zawar-Reza, P., Sturman, A., Alizadeh Choobari, O., Zawar-Reza, P., & Sturman, A. (2014). The global distribution of mineral dust and its impacts on the climate system: A review. *Atmospheric Research*, *138*, 152–165. https://doi.org/10.1016/j.atmosres.2013.11.007

Anderson, W., Cook, B. I., Slinski, K., Schwarzwald, K., McNally, A., & Funk, C. (2022). Multi-year La Niña events and multi-season drought in the Horn of Africa. *Journal of Hydrometeorology*, *1–24*, 119–131. https://doi.org/10.1175/JHM-D-22-0043

Ashpole, I., & Washington, R. (2012). An automated dust detection using SEVIRI: A multiyear climatology of summertime dustiness in the central and Western Sahara. *Journal of Geophysical Research*, *117*(D8), D08202. https://doi.org/10.1029/2011JD016845

Bakker, N. L., Drake, N. A., & Bristow, C. S. (2019). Evaluating the relative importance of northern African mineral dust sources using remote sensing. *Atmospheric Chemistry and Physics*, *19*(16), 10525–10535. https://doi.org/10.5194/acp-19-10525-2019

Banks, J. R., Hünerbein, A., Heinold, B., Brindley, H. E., Deneke, H., & Schepanski, K. (2019). The sensitivity of the colour of dust in MSG-SEVIRI Desert Dust infrared composite imagery to surface and atmospheric conditions. *Atmospheric Chemistry and Physics*, *19*(10), 6893–6911. https://doi.org/10.5194/acp-19-6893-2019

Banks, J. R., Schepanski, K., Heinold, B., Hünerbein, A., & Brindley, H. E. (2018). The influence of dust optical properties on the colour of simulated MSG-SEVIRI Desert Dust infrared imagery. *Atmospheric Chemistry and Physics*, *18*(13), 9681–9703. https://doi.org/10.5194/acp-18-9681-2018

Bauduin, D., Moniod, F., Bermond, G., Jarre, P., Le Duc, P., Robin, J., & Sabatier, J. (1973). Wabi Shebelle Survey: Hydrological survey of the Wabi Shebelle basin. *Imp. Ethiop. Gov. Natl. Water Resour. Com.*

Beguería, S., Vicente-Serrano, S. M., Reig, F., & Latorre, B. (2014). Standardized precipitation evapotranspiration index (SPEI) revisited: Parameter fitting, evapotranspiration models, tools, datasets and drought monitoring. *International Journal of Climatology*, *34*(10), 3001–3023. https://doi.org/10.1002/joc.3887

Behera, S. K., Luo, J. J., Masson, S., Rao, S. A., Sakuma, H., & Yamagata, T. (2006). A CGCM study on the interaction between IOD and ENSO. *Journal of Climate*, *19*(9), 1688–1705. https://doi.org/10.1175/JCLI3797.1

Beyene, A., & Abdelsalam, M. G. (2005). Tectonics of the Afar depression: A review and synthesis. *Journal of African Earth Sciences*, *41*(1–2), 41–59. https://doi.org/10.1016/j.jafrearsci.2005.03.003

Billi, P. (2015). *Landscapes and landforms of Ethiopia*. Springer Dordrecht. https://doi.org/10.1007/978-94-017-8026-1

Billi, P. (2022a). Climate variability in the Horn of Africa eastern countries: Eritrea, Djibouti, Somalia. In P. Billi (Ed.), *Landscapes and landforms of the Horn of Africa: Eritrea, Djibouti, Somalia* (pp. 185–199). Springer International Publishing AG.

Billi, P. (2022b). Fluvial landscape of the Dabaan basin, northern Somalia. In *Landscapes and landforms of the Horn of Africa: Eritrea* (pp. 265–280).

Biswas, A. K., Masakhalia, Y. F. O., Odero-Ogwel, L. A., & Pallangyo, E. P. (1987). Land use and farming systems in the Horn of Africa. *Land Use Policy*, *4*, 419–443. https://doi.org/10.1016/0264-8377(87)90064-0

Breeze, P. S., Drake, N. A., Groucutt, H. S., Parton, A., Jennings, R. P., White, T. S., et al. (2015). Remote sensing and GIS techniques for reconstructing Arabian palaeohydrology and identifying archaeological sites. *Quaternary International*, *382*, 98–119. https://doi.org/10.1016/j.quaint.2015.01.022

Brooks, N., & Legrand, M. (2000). Dust variability over northern Africa and rainfall in the Sahel 1–25. https://doi.org/10.1007/0-306-48086-7_1

Buchhorn, M., Lesiv, M., Tsendbazar, N.-E., Herold, M., Bertels, L., & Smets, B. (2020). Copernicus global land cover layers — Collection 2. *Remote Sensing*, *108*(6), 1044. https://doi.org/10.3390/rs12061044

Carlson, T. N. (1979). Atmospheric turbidity in Saharan dust outbreaks as determined by analyses of satellite brightness data. *Monthly Weather Review*, *107*(3), 322–335. https://doi.org/10.1175/1520-0493(1979)107<0322:atisdo>2.0.co;2

Clemens, S. C., Murray, D. W., & Prell, W. L. (1996). Nonstationary phase of the Plio-Pleistocene Asian monsoon. *Science (80-.)*, *274*(5289), 943–948. https://doi.org/10.1126/science.274.5289.943

Crocker, A. J., Naafs, B. D. A., Westerhold, T., James, R. H., Cooper, M. J., Röhl, U., et al. (2022). Astronomically controlled aridity in the Sahara since at least 11 million years ago. *Nature Geoscience*, *15*(8), 671–676. https://doi.org/10.1038/s41561-022-00990-7

Davis, S. R., Farrar, J. T., Weller, R. A., Jiang, H., & Pratt, L. J. (2019). The land-sea breeze of the Red Sea: Observations, simulations, and relationships to regional moisture transport. *Journal of Geophysical Research: Atmospheres*, *124*(24), 13803–13825. https://doi.org/10.1029/2019JD031007

deMenocal, P. B. (1995). Plio-Pleistocene African climate. *Science (80-.)*, *270*(5233), 53–59. https://doi.org/10.1126/science.270.5233.53

deMenocal, P. B. (2004). African climate change and faunal evolution during the Pliocene - Pleistocene. *Earth and Planetary Science Letters*, *220*(1–2), 3–24. https://doi.org/10.1016/S0012-821X(04)00003-2

Didan, K. (2015). MOD13Q1 MODIS/Terra vegetation indices 16-day L3 global 250m SIN grid V006. Distrib. By NASA EOSDIS L. Process. *DAAC*. https://doi.org/10.5067/MODIS/MOD13Q1.006

Esmaeil, N., Gharagozloo, M., Rezaei, A., & Grunig, G. (2014). Dust events, pulmonary diseases and immune system. *African Journal of Clinical and Experimental Immunology*, *3*, 20.

Fazzini, M., Bisci, C., & Billi, P. (2015). The climate of Ethiopia. In P. Billi (Ed.), *Landscapes and landforms of Ethiopia* (pp. 65–87). Springer.

Fenta, A. A., Tsunekawa, A., Haregeweyn, N., Poesen, J., Tsubo, M., Borrelli, P., et al. (2020). Land susceptibility to water and wind erosion risks in the East Africa region. *Science of the Total Environment*, *703*, 135016. https://doi.org/10.1016/j.scitotenv.2019.135016

FEWS NET. (2007). Famine early warning systems network [WWW document]. *USAIDS*. Retrieved from https://fews.net

Fiedler, S., Schepanski, K., Heinold, B., Knippertz, P., & Tegen, I. (2013). Climatology of nocturnal low-level jets over North Africa and implications for modeling mineral dust emission. *Journal of Geophysical Research: Atmospheres*, *118*(12), 6100–6121. https://doi.org/10.1002/jgrd.50394

Fuell, K., Guyer, B., Kann, D., Molthan, A., & Elmer, N. (2016). Next generation satellite RGB dust imagery leads to operational changes at NWS Alburquerque. *Journal of Operational Meteorology*, *04*(06), 75–91. https://doi.org/10.15191/nwajom.2016.0406

Funk, C., Dettinger, M. D., Michaelsen, J. C., Verdin, J. P., Brown, M. E., Barlow, M., & Hoell, A. (2008). Warming of the Indian Ocean threatens eastern and southern African food security but could be mitigated by agricultural development. *Proceedings of the National Academy of Sciences of the United States of America*, *105*(32), 11081–11086. https://doi.org/10.1073/pnas.0708196105

Funk, C., Peterson, P., Landsfeld, M., Pedreros, D., Verdin, J., Shukla, S., et al. (2015). The climate hazards infrared precipitation with stations - a new environmental record for monitoring extremes. *Scientific Data*, *2*, 1–21. https://doi.org/10.1038/sdata.2015.66

Gasse, F. (1974). Diatoms of the holocene sediments in the Afrera lake basin (northern Afar, Ethiopia). *Internationale Revue der Gesamten Hydrobiologie*, *59*(1), 95–122. https://doi.org/10.1002/iroh.19740590112

Gherboudj, I., Naseema Beegum, S., & Ghedira, H. (2017). Identifying natural dust source regions over the Middle-East and North-Africa: Estimation of dust emission potential. *Earth-Science Reviews*, *165*, 342–355. https://doi.org/10.1016/j.earscirev.2016.12.010

Ginoux, P., Prospero, J. M., Gill, T. E., Hsu, N. C., & Zhao, M. (2012). Global-scale attribution of anthropogenic and natural dust source and their emission rates based on MODIS deep blue aerosol products. *Reviews of Geophysics*, *50*(3), 1–36. https://doi.org/10.1029/2012RG000388

Hafez, Y. (2016). Study on the relationship between the oceanic Nino index and surface air temperature and precipitation rate over the Kingdom of Saudi Arabia. *Journal of Geoscience and Environment Protection*, *4*(5), 146–162. https://doi.org/10.4236/gep.2016.45015

Haile, G. G., Tang, Q., Sun, S., Huang, Z., Zhang, X., & Liu, X. (2019). Droughts in east Africa: Causes, impacts and resilience. *Earth-Science Reviews*, *193*, 146–161. https://doi.org/10.1016/j.earscirev.2019.04.015

Hennen, M. (2017). *Characterisation of mineral dust emission in the Middle East using remote sensing techniques*. University of Reading.

Hennen, M., White, K., & Shahgedanova, M. (2019). An assessment of SEVIRI imagery at various temporal resolutions and the effect on accurate dust emission mapping. *Remote Sensing*, *11*(8), 918. https://doi.org/10.3390/rs11080918

Herman, J. R., Bhartia, P. K., Torres, O., Hsu, C., Seftor, C., & Celarier, E. (1997). Global distribution of UV-absorbing aerosols from Nimbus 7/TOMS data. *Journal of Geophysical Research*, *102*(D14), 16911–16922. https://doi.org/10.1029/96jd03680

Hession, S. L., & Moore, N. (2011). A spatial regression analysis of the influence of topography on monthly rainfall in East Africa. *International Journal of Climatology*, *31*(10), 1440–1456. https://doi.org/10.1002/joc.2174

Hsu, N. C., Tsay, S. C., King, M. D., & Herman, J. R. (2004). Aerosol properties over bright-reflecting source regions. *IEEE Transactions on Geoscience and Remote Sensing*, *42*(3), 557–569. https://doi.org/10.1109/TGRS.2004.824067

Huneeus, N., Schulz, M., Balkanski, Y., Griesfeller, J., Prospero, J., Kinne, S., et al. (2011). Global dust model intercomparison in AeroCom phase i. *Atmospheric Chemistry and Physics*, *11*(15), 7781–7816. https://doi.org/10.5194/acp-11-7781-2011

Jewell, A. M., Drake, N., Crocker, A. J., Bakker, N. L., Kunkelova, T., Bristow, C. S., et al. (2021). Three North African dust source areas and their geochemical fingerprint. *Earth and Planetary Science Letters*, *554*, 116645. https://doi.org/10.1016/j.epsl.2020.116645

Jickells, T. D., An, Z. S., Andersen, K. K., Baker, A. R., Bergametti, G., Brooks, N., et al. (2005). Global iron connections between desert dust, ocean biogeochemistry, and climate. *Science (80-.)*, *308*(5718), 67–72. https://doi.org/10.1126/science.1105959

Kajtar, J. B., Santoso, A., England, M. H., & Cai, W. (2017). Tropical climate variability: Interactions across the Pacific, Indian, and Atlantic oceans. *Climate Dynamics*, *48*(7–8), 2173–2190. https://doi.org/10.1007/s00382-016-3199-z

Khan, B., Abualnaja, Y., Al-Subhi, A. M., Nellayaputhenpeedika, M., Nellikkattu Thody, M., & Sturman, A. P. (2018). Climatology of sea breezes along the Red Sea coast of Saudi Arabia. *International Journal of Climatology*, *38*(9), 3633–3650. https://doi.org/10.1002/joc.5523

Knippertz, P., Deutscher, C., Kandler, K., Müller, T., Schulz, O., & Schütz, L. (2007). Dust mobilization due to density currents in the Atlas region: Observations from the Saharan Mineral Dust Experiment 2006 field campaign. *Journal of Geophysical Research*, *112*(D21), 1–14. https://doi.org/10.1029/2007JD008774

Knippertz, P., & Todd, M. C. (2012). Mineral dust aerosols over the Sahara: Meteorological controls on emission and transport and implications for modeling. *Reviews of Geophysics*, *50*(1), RG1007. https://doi.org/10.1029/2011RG000362

Kok, J. F., Ward, D. S., Mahowald, N. M., & Evan, A. T. (2018). Global and regional importance of the direct dust-climate feedback. *Nature Communications*, *9*(1), 241. https://doi.org/10.1038/s41467-017-02620-y

Krishnamurthy, P. K., Choularton, R. J., & Kareiva, P. (2020). Dealing with uncertainty in famine predictions: How complex events affect food security early warning skill in the Greater Horn of Africa. *Global Food Security*, *26*, 100374. https://doi.org/10.1016/j.gfs.2020.100374

Kunkelova, T., Crocker, A. J., Jewell, A. M., Breeze, P. S., Drake, N. A., Cooper, M. J., et al. (2022). Dust sources in Westernmost Asia have a different geochemical fingerprint to those in the Sahara. *Quaternary Science Reviews*, *294*, 107717. https://doi.org/10.1016/j.quascirev.2022.107717

Lal, R. (2014). Sustainable intensification for adaptation and mitigation of climate change and advancement of food security in Africa. In *Sustainable intensification to advance food security and enhance climate resilience in Africa* (pp. 3–17). https://doi.org/10.1007/978-3-319-09360-4_1

Lehner, B., Verdin, K., & Jarvis, A. (2008). New global hydrography derived from spaceborne elevation data. *Eos*, *89*(10), 93–94. https://doi.org/10.1029/2008EO100001

Liebmann, B., Hoerling, M. P., Funk, C., Bladé, I., Dole, R. M., Allured, D., et al. (2014). Understanding recent eastern Horn of Africa rainfall variability and change. *Journal of Climate*, *27*(23), 8630–8645. https://doi.org/10.1175/JCLI-D-13-00714.1

Lohmann, U., & Feichter, J. (2005). Global indirect aerosol effects: A review. *Atmospheric Chemistry and Physics*, *5*(3), 715–737. https://doi.org/10.5194/acp-5-715-2005

Lyon, B., & Dewitt, D. G. (2012). A recent and abrupt decline in the East African long rains. *Geophysical Research Letters*, *39*(2), 1–5. https://doi.org/10.1029/2011GL050337

Mahowald, N. M. (2007). Anthropocene changes in desert area: Sensitivity to climate model predictions. *Geophysical Research Letters*, *34*(18), 1–5. https://doi.org/10.1029/2007GL030472

Manning, K., Breeze, P. S., Drake, N., Dunne, J., Casanova, E., & Evershed, R. P. (2023). Habitat fragmentation and the sporadic spread of pastoralism in the mid-holocene Sahara. *Quaternary Science Reviews*, *309*, 108070. https://doi.org/10.1016/j.quascirev.2023.108070

McGee, D., de Menocal, P. B., Winckler, G., Stuut, J. B. W., & Bradtmiller, L. I. (2013). The magnitude, timing and abruptness of changes in North African dust deposition over the last 20,000 yr. *Earth and Planetary Science Letters*, *371–372*, 163–176. https://doi.org/10.1016/j.epsl.2013.03.054

Mège, D., Purcell, P., Pochat, S., & Guidat, T. (2015). The landscape and landforms of the Ogaden, southeast Ethiopia. In *Landscapes and landforms of Ethiopia* (pp. 323–348).

Mekonnen, A., & Rossow, W. B. (2018). The interaction between deep convection and easterly wave activity over Africa: Convective transitions and mechanisms. *Monthly Weather Review*, *146*(6), 1945–1961. https://doi.org/10.1175/MWR-D-17-0217.1

Merla, G., Abbate, E., Canuti, P., Sagri, M., & Tacconi, P. (1973). *A geological map of Ethiopia and Somalia. 1:2,000,000*. Cons. Naz. delle Ric. Italy.

Miller, S. D., Kuciauskas, A. P., Liu, M., Ji, Q., Reid, J. S., Breed, D. W., et al. (2008). Haboob dust storms of the southern Arabian Peninsula. *Journal of Geophysical Research*, *113*(D1), 1–26. https://doi.org/10.1029/2007JD008550

Miller, S. T. K., Keim, B. D., Talbot, R. W., & Mao, H. (2003). Sea breeze: Structure, forecasting, and impacts. *Reviews of Geophysics*, *41*(3), 1011. https://doi.org/10.1029/2003RG000124

Morton, J. F. (2007). The impact of climate change on smallholder and subsistence agriculture. *Proceedings of the National Academy of Sciences of the United States of America*, *104*(50), 19680–19685. https://doi.org/10.1073/pnas.0701855104

Mpelasoka, F., Awange, J. L., & Zerihun, A. (2018). Influence of coupled ocean-atmosphere phenomena on the greater Horn of Africa droughts and their implications. *Science of the Total Environment*, *610–611*, 691–702. https://doi.org/10.1016/j.scitotenv.2017.08.109

Mulitza, S., Prange, M., Stuut, J. B. W., Zabel, M., Von Dobeneck, T., Itambi, A. C., et al. (2008). Sahel megadroughts triggered by glacial slowdowns of Atlantic meridional overturning. *Paleoceanography*, *23*(4), 1–11. https://doi.org/10.1029/2008PA001637

Munday, C., Savage, N., Jones, R. G., & Washington, R. (2023). Valley formation aridifies East Africa and elevates Congo Basin rainfall. *Nature*, *615*(7951), 276–279. https://doi.org/10.1038/s41586-022-05662-5

Muñoz Sabater, J. (2019). *ERA5-Land monthly averaged data from 1981 to present [WWW Document]*. Copernicus Clim. Chang. Serv. Clim. Data Store (CDS). https://doi.org/10.24381/cds.68d2bb3

Nicholson, S. E. (1996). A review of climate dynamics and climate variability in eastern Africa. In *The limnology, climatology and paleoclimatology of the East African lakes* (pp. 25–56). https://doi.org/10.1201/9780203748978-2

Nicholson, S. E. (2017). Climate and climatic variability of rainfall over eastern Africa. *Reviews of Geophysics*, *55*(3), 590–635. https://doi.org/10.1002/2016RG000544

Parajuli, S. P., & Zender, C. S. (2017). Connecting geomorphology to dust emission through high-resolution mapping of global land cover and sediment supply. *Aeolian Research*, *27*, 47–65. https://doi.org/10.1016/j.aeolia.2017.06.002

Pedgley, D. E. (1967). Air temperature at Dallol Ethiopia. *The Meteorological Magazine*, *96*, 265.

Prospero, J. M. (1981). Arid regions as sources of mineral aerosols in the marine atmosphere. *Special Papers - Geological Society of America*, *186*, 71–86. https://doi.org/10.1130/SPE186-p71

Prospero, J. M., Ginoux, P., Torres, O., Nicholson, S. E., & Gill, T. E. (2002). Environmental characterization of global sources of atmospheric soil dust identified with the Nimbus 7 Total Ozone Mapping Spectrometer (TOMS) absorbing aerosol product. *Reviews of Geophysics*, *40*, 1–31. https://doi.org/10.1029/2000RG000095

Rayner, N. A., Parker, D. E., Horton, E. B., Folland, C. K., Alexander, L. V., Rowell, D. P., et al. (2003). Global analyses of sea surface temperature, sea ice, and night marine air temperature since the late nineteenth century. *Journal of Geophysical Research*, *108*(D14), 4407. https://doi.org/10.1029/2002jd002670

Saji, N. H., Goswami, B., Vinayachandran, P., & Yamagata, T. (1999). A dipole mode in the Tropical Ocean. *Nature*, *401*(6751), 360–363. https://doi.org/10.1038/43854

Saji, N. H., & Yamagata, T. (2003). Possible impacts of Indian Ocean Dipole mode events on global climate. *Climate Research*, *25*, 151–169. https://doi.org/10.3354/cr025151

Schepanski, K., Flamant, C., Chaboureau, J. P., Kocha, C., Banks, J. R., Brindley, H. E., et al. (2013). Characterization of dust emission from alluvial sources using aircraft observations and high-resolution modeling. *Journal of Geophysical Research: Atmospheres*, *118*(13), 7237–7259. https://doi.org/10.1002/jgrd.50538

Schepanski, K., Heinold, B., & Tegen, I. (2017). Harmattan, Saharan heat low, and west African monsoon circulation: Modulations on the Saharan dust outflow towards the North Atlantic. *Atmospheric Chemistry and Physics*, *17*, 10223–10243. https://doi.org/10.5194/acp-17-10223-2017

Schepanski, K., Tegen, I., Laurent, B., Heinold, B., & Macke, A. (2007). A new Saharan dust source activation frequency map derived from MSG-SEVIRI IR-channels. *Geophysical Research Letters*, *34*(18), 1–5. https://doi.org/10.1029/2007GL030168

Schepanski, K., Tegen, I., & Macke, A. (2012). Comparison of satellite based observations of Saharan dust source areas. *Remote Sensing of Environment*, *123*, 90–97. https://doi.org/10.1016/j.rse.2012.03.019

Schepanski, K., Tegen, I., Todd, M. C., Heinold, B., Bönisch, G., Laurent, B., & Macke, A. (2009). Meteorological processes forcing Saharan dust emission inferred from MSG-SEVIRI observations of subdaily dust source activation and numerical models. *Journal of Geophysical Research*, *114*(D10), 1–18. https://doi.org/10.1029/2008JD010325

Seife, T. K. (2021). The impact of climate change on agriculture and food security in the greater Horn of Africa. *Politikon*, *48*(1), 98–114. https://doi.org/10.1080/02589346.2020.1861509

Shao, Y., Wyrwoll, K. H., Chappell, A., Huang, J., Lin, Z., McTainsh, G. H., et al. (2011). Dust cycle: An emerging core theme in Earth system science. *Aeolian Research*, *2*(4), 181–204. https://doi.org/10.1016/j.aeolia.2011.02.001

Sokolik, I. N. (2002). The spectral radiative signature of wind-blown mineral dust: Implications for remote sensing in the thermal IR region. *Geophysical Research Letters*, *29*(24), 2–5. https://doi.org/10.1029/2002GL015910

Sokolik, I. N., & Toon, O. B. (1996). Direct radiative forcing by anthropogenic airborne mineral aerosols. *Nature*, *381*(6584), 681–683. https://doi.org/10.1038/381681a0

Sokolik, I. N., Winker, D. M., Bergametti, G., Gillette, D. A., Carmichael, Y. J., Kaufman, Y. J., et al. (2001). Introduction to special section: Outstanding problems in quantifying the radiative impacts of mineral dust. *Journal of Geophysical Research*, *106*(D16), 18015–18027. https://doi.org/10.1029/2000jd900498

Sutton, L. J. (1925). Haboobs. *Quarterly Journal of the Royal Meteorological Society*, *51*(213), 25–30. https://doi.org/10.1002/qj.49705121305

Tam, W. W. S., Wong, T. W., Wong, A. H. S., & Hui, D. S. C. (2012). Effect of dust storm events on daily emergency admissions for respiratory diseases. *Respirology*, *17*(1), 143–148. https://doi.org/10.1111/j.1440-1843.2011.02056.x

Tegen, I., Werner, M., Harrison, S. P., & Kohfeld, K. E. (2004). Relative importance of climate and land use in determining present and future global soil dust emission. *Geophysical Research Letters*, *31*(5), L05105. https://doi.org/10.1029/2003gl019216

Tierney, J. E., Ummenhofer, C. C., & de Menocal, P. B. (2015). Past and future rainfall in the Horn of Africa. *Science Advances*, *1*(9), e1500682. https://doi.org/10.1126/sciadv.1500682

Tola, S. Y., & Shetty, A. (2021). Land cover change and its implication to hydrological regimes and soil erosion in Awash River basin, Ethiopia: A systematic review. *Environmental Monitoring and Assessment*, *193*(12), 836. https://doi.org/10.1007/s10661-021-09599-6

Torres, O., Bhartia, P. K., Herman, J. R., Ahmad, Z., & Gleason, J. (1998). Derivation of aerosol properties from satellite measurements of backscattered ultraviolet radiation: Theoretical basis. *Journal of Geophysical Research*, *103*(D14), 17099–17110. https://doi.org/10.1029/98JD02709

Torres, O., Bhartia, P. K., Herman, J. R., Sinyuk, A., Ginoux, P., & Holben, B. (2002). A long-term record of aerosol optical depth from TOMS observations and comparison to AERONET measurements. *Journal of the Atmospheric Sciences*, *59*(3), 398–413. https://doi.org/10.1175/1520-0469(2002)059<0398:altroa>2.0.co;2

Torres, O., Tanskanen, A., Veihelmann, B., Ahn, C., Braak, R., Bhartia, P. K., et al. (2007). Aerosols and surface UV products form Ozone Monitoring Instrument observations: An overview. *Journal of Geophysical Research*, *112*(D24), 1–14. https://doi.org/10.1029/2007JD008809

Van den Hende, C., Van Schaeybroeck, B., Nyssen, J., Van Vooren, S., Van Ginderachter, M., & Termonia, P. (2021). Analysis of rain-shadows in the Ethiopian Mountains using climatological model data. *Climate Dynamics*, *56*(5–6), 1663–1679. https://doi.org/10.1007/s00382-020-05554-2

Varet, J. (2018). *Geology of Afar (east Africa)*. Springer Cham. https://doi.org/10.1007/978-3-319-60865-5

Viste, E., & Sorteberg, A. (2013). Moisture transport into the Ethiopian highlands. *International Journal of Climatology*, *33*(1), 249–263. https://doi.org/10.1002/joc.3409

Washington, R., Todd, M., Middleton, N. J., & Goudie, A. S. (2003). Dust-storm source areas determined by the total ozone monitoring spectrometer and surface observations. *Annals of the Association of American Geographers*, *93*(2), 297–313. https://doi.org/10.1111/1467-8306.9302003

Washington, R., Todd, M. C., Engelstaedter, S., Mbainayel, S., & Mitchell, F. (2006). Dust and the low-level circulation over the Bodélé depression, Chad: Observations from BoDEx 2005. *Journal of Geophysical Research*, *111*(D3), 1–15. https://doi.org/10.1029/2005JD006502

Webb, N. P., & Strong, C. L. (2011). Soil erodibility dynamics and its representation for wind erosion and dust emission models. *Aeolian Research*, *3*(2), 165–179. https://doi.org/10.1016/j.aeolia.2011.03.002

Williams, A. P., & Funk, C. (2011). A westward extension of the warm pool leads to a westward extension of the Walker circulation, drying eastern Africa. *Climate Dynamics*, *37*(11–12), 2417–2435. https://doi.org/10.1007/s00382-010-0984-y

Woodward, S., Roberts, D. L., & Betts, R. A. (2005). A simulation of the effect of climate change-induced desertification on mineral dust aerosol. *Geophysical Research Letters*, *32*(18), 1–4. https://doi.org/10.1029/2005GL023482

Wu, M., Liu, X., Yu, H., Wang, H., Shi, Y., Yang, K., et al. (2020). Understanding processes that control dust spatial distributions with global climate models and satellite observations. *Atmospheric Chemistry and Physics*, *20*(22), 13835–13855. https://doi.org/10.5194/acp-20-13835-2020

Wurzler, S., Reisin, T. G., & Levin, Z. (2000). Modification of mineral dust particles by cloud processing and subsequent effects on drop size distributions. *Journal of Geophysical Research*, *105*(D4), 4501–4512. https://doi.org/10.1029/1999JD900980